University of Nevada, Reno

Novel Design of Low Power Device for Measurement and Conversion of Continuous Cellular Pulse-Rate Signal to Optical for Potential Use in Implantable Devices

A thesis submitted in partial fulfillment of the requirements for the degree of

Master of Science in Biomedical Engineering

By

Matthew Henderson

Dr. Ji Hwan Yoon / Thesis Advisor

May 2022

THE GRADUATE SCHOOL

We recommend that the thesis
prepared under our supervision by

Matthew Henderson

entitled

Novel Design of Low Power Device for Measurement and Conversion of Continuous Cellular Pulse-Rate Signal to Optical for Potential Use in Implantable Devices

be accepted in partial fulfillment of the
requirements for the degree of

Master of Science

Ji Hwan Yoon
Advisor

Banmali Rawat
Committee Member

Josette El Zaklit
Committee Member

Sal Baker
Graduate School Representative

David W. Zeh, Ph.D., Dean
Graduate School

May, 2022

Abstract

Implantable devices have become increasingly commonplace as the technologies of electronic component manufacturing have allowed engineers to develop increasingly more capable devices at small scale. These devices are designed to survive the unique environment of the body. These design requirements must include being small enough to be implanted in their desired region of the body, as well as proper shielding from the noise of the activity of the surrounding tissues, and not having a negative effect on the health and function of the tissue surrounding the device. Light is an ideal medium for transduction of signals within an implantable device placed in the human body, as there are very few optically sensitive tissues, such as those of the eye. In an enclosed device no tissue activity within the body poses a risk of interference for optical signals.

Implantable devices have historically served many purposes ranging from regulation devices such as pacemakers to supplemental roles like those of the artificial pancreas. Continuing this trend, the supplement or replacement of damaged nerves could be achieved by the design of a small, implantable device capable of amplifying the signal of nerves in damaged regions and converting them to a medium of transmission not prone to, or the cause of, interference within the body. To this end, this thesis will outline the design of a small device capable of amplifying bioelectric signals to a level wherein conversion to optically modulated signal is achieved.

Acknowledgements

I am hugely appreciative to all of the phenomenal educators I have had through my entire academic career for their unwavering faith in their students and in demonstrating the real value of education. To Mrs. Spence and Mrs. Lacombe, thank you for teaching me about how huge the universe is, I will never forget the planets. To Mrs. Ellen Minetto, thank you for showing me the value of curiosity and music. To Mrs. Diana Garrity, thank you for pushing all of us to pursue our passions to our fullest and to see our projects through. To Mrs. Gorham, thank you for always showing that science will always have the answers if we're willing to look for them. To Ms. Walenta, thank you for showing us the wonder of all things big and small. To Senora Hatjakes, I cannot put into words how helpful it has been to have another language, thank you.

To my non-academic instructors, I owe much to my instructors Grand Master Lawrence Cary and Master Scott Forsythe, for pushing me to find new limits and then pass them, as well for showing me that the truest show of mastery over a subject, is the ability to teach it. To Adam Yarnes, I owe you a great deal for showing me the value of patience, helping others through education, and the beauty of the natural world. I hope to have even a fraction of the positive impact that you continue to have on the world, and I cannot express how valuable your lessons have been. I wish you all the best, and good health.

Lastly, I would like to thank the professors who have shown me the most important information about my research and given me the tools and knowledge I need to

make this project a reality. To Dr. Banmali Rawat, thank you for your extensive knowledge of electromagnetic materials and behaviors, and optical fiber technology. I hope to carry on your message that the future of technology is optical in my career. To Dr. Josette El Zaklit, thank you for your great insight into the working of bioelectricity. To Dr. Sal Baker and his students Dante and Peter, thank you for sharing your experience and materials in tissue science and how they are recorded. I would also like to thank Dr. Bahram Parvin and Dr. Qingsu Chen, for giving me the resources and knowledge very early in my undergraduate career that would allow me to conduct proper research. Thank you to Vasilii Mansurov for helping me at every step of the process, including the fabrication and part searches that made this project possible. Thank you to Dr. Gould and his student Farhana for sharing your lab and tissue materials as well, it was immensely helpful and appreciated.

Table of Contents

List of Tables

Chapter 1

List of Figures

Chapter 1

Chapter 2

Chapter 3

Chapter 4

Chapter 1

Overview and Introduction

Introduction

Microneurography was a major breakthrough of the early 20th century that would allow researchers to observe the individual impulse signals of neurons within peripheral nerve tissue [1]. Over the following decades, many advances to materials and amplification techniques would allow for the visualization of individual impulse events measured within the body, as well as distinct impulse data from both efferent and afferent nerves involving highly specified neural structures such as merkel cells [4]. These electrical pulse trains occur as a result of depolarization within neuronal membranes, raising the resting potential of -70mV to around 35mV for most neurons. This action potential depolarization phase is caused mainly by the influx of sodium into the neuronal cells, though many central nervous system nerves will also utilize calcium and chlorine in their propagation of neuronal signals, utilizing both electrical and chemical signaling between tissues. More recent biological signal analysis tools such as calcium imaging have given further insight into the electrical activity within tissues such as neuronal, cardiac and gastrointestinal muscles. These imaging techniques allow for the monitoring of ionic charges being carried by cellular membranes along lengths of tissues as they propagate and cause tissue responses like contractions necessary for digestion [6].

Regarding the electrical signals of excitable tissues, signal amplification and filtration have been critical to allow proper capture. While the measured voltage potential of neuron membranes is reported in the mV range, many microneurography techniques record these signals in the μV range for higher temporal clarity and the trade-off is signal sensitivity [2]. This type of recordings requires many biosensors, extreme degrees of filtering and noise reduction protocols. This can be achieved through strictly controlled amplification parameters, bandpass filters tailored to the particular frequencies of impulse trains, and elements that respond to changes in membrane capacitance and resistance as a result of changes to membrane structures during probing. It is also imperative that these biosensor components do not generate any signal that will interfere with any of the signals being measured, and as such passive probe components are ideal for this application.

Implantable devices must also be made in a way that prevents biological reactions that reject devices. Traditionally, coatings and specialized metal alloys have been used such as those in metal joint replacements, however, even these can erode over time. With this in mind, the inert materials used in both the cable and coatings of the optical fiber may prove an ideal candidate for biomedical device implantation. In many cases, optical fiber can be made with a non-corroding, inert combination of indium, gallium, germanium, and/or silicon, the latter of which is already used in many commonly implemented devices and proven to be safe [9].

Optical fiber utilization in communication applications is designed specifically to transmit impulse train information in the form of light fired from laser diodes within communication circuits. This light is modulated in response to input signals, varying the intensity of the light that can then be reconverted back to electrical signals for data collection. This fiber is also extremely small, often in the micrometer range at the core of single-mode fiber, which itself is capable of transmitting information of substantially higher density than the calculated information density of neuronal electrical impulse trains [9][3].

Microneurography and Neural Impulse Trains

The practice of microneurography involves a few key components, namely the careful placement of tungsten needle electrodes, usually in the range of 100-200 micrometers thick with a 1 micrometer tip. These probes can be placed freely into flesh for bodily use with no lasting damage demonstrated after correct placement [5]. The tips of these probes are placed directly into the nerve fascicles of myelinated and unmyelinated nerves, taking recordings of the electrical signal activity to be amplified at later stages [7]. Different types of neurons, more specifically types of somatic endings, have been demonstrated as having distinct electrical impulse patterns. Figure 1.1 shows distinctions between cutaneous mechanoreceptors, including their location and impulse responses. Low threshold mechanoreceptors (LTMR) demonstrate a wide range of responses including repeated pulses and dipole pulses possibly signifying on/off responses like those seen in meissner corpuscle stimulation [4]. High threshold mechanoreceptors (HTMR) are only stimulated in the presence of noxious mechanical pressure, which then triggers a response from nociceptors further into the nerve for sensing pain [4].

Physiological subtype	Associated fiber (conduction velocity[1])	Skin type	End organ/ending type	Location	Optimal Stimulus[4]	Response properties
SAI-LTMR	Ab (16–96m/s)	Glabrous	Merkel cell	Basal Layer of epidermis	Indentation	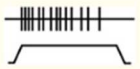
		Hairy	Merkel cell (touch dome)	Around Guard hair follicles		
SAII-LTMR	Ab (20–100m/s)	Glabrous	Ruffini[2]	Dermis[3]	Stretch	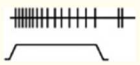
		Hairy	unclear	unclear		
RAI-LTMR	Ab (26–91m/s)	Glabrous	Meissner corpuscle	Dermal papillae	Skin movement Hair follicle deflection	
		Hairy	Longitudinal lanceolate ending	Guard/Awl-Auchene hair follicles		
RAII-LTMR	Ab (30–90m/s)	Glabrous	Pacinian corpuscle	Deep dermis	Vibration	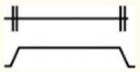
Ad-LTMR	Ad (5–30m/s)	Hairy	Longitudinal lanceolate ending	Awl-Auchene/ Zigzag hair follicles	Hair follicle deflection	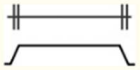
C-LTMR	C (0.2–2m/s)	Hairy	Longitudinal lanceolate ending	Awl-Auchene/ Zigzag hair follicles	Hair follicle deflection	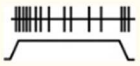
HTMR	Ab/Ad/C (0.5–100m/s)	Glabrous Hairy	Free nerve ending	Epidermis/Dermis	Noxious mechanical	

Table 1.1: Comparison of Cutaneous Mechanoreceptors [4]

These impulse trains are not specific to somatic endings though, and also control signals to motor endplates in afferent nerves for muscle control [5]. In cases of mammalian neuromuscular junction, these afferent impulses also trigger the

release of signaling molecules like acetylcholine or calcium at their endplates, meaning that impulses must be measured at a position on the nerve prior to intersection with the neuromuscular junction [7].

Bioelectric measurements are often gathered at such small voltage ranges that measurement without amplification becomes extremely impractical. The process of taking these measurements relies on the observation of very specific ionic activity across the membrane resulting in action potentials, which create a measurable spike in charge across the membrane [2]. Therefore, many special amplification procedures exist to make this impulse train detectable for data collection. Primarily, this involves the creation of a bio-signal amplifier with an extremely high signal to noise ratio, levels of filtering, use of passive elements in any probing devices, and electronics capable of acting on extremely low input currents [1].

Patch Clamp Amplification

In many cases, amplification of bioelectric signals utilize a very large external amplifier meant to provide several layers of filtration and signal isolation to gather specific information regarding changes in membrane voltages, rise and fall times of membrane charge potentials, and ion exchange along the measured membranes [8]. The size and power consumption of these external amplifiers however proves impractical in the case of bodily implants for biomedical devices. To this end, redesign of bioamplification devices to reduce both of these factors should be explored. Patch clamp amplification has been achieved at millimeter scale by etching individual components directly into silicon [8]. Patch clamp measurement techniques are only used for medical research, as they require access to cell membranes to allow measurements of cellular currents and voltage, The method requires cell isolation from tissues and this may result in loss of key proteins and cell damage [10]. The amplification used in this method however, proves capable of amplifying signals initially measured at miniscule levels, and has become a staple in fields requiring bioelectric measurement at cellular activity [10]. For this reason, patch clamp amplifiers should be modified to achieve the small scales required for biomedical implant use cases.

To keep measurements consistent, factors relating to the physical characteristics of the cell membrane must be taken into account for the proper design of an amplification circuit. Changes to the innate resistance and capacitance of the membrane can occur, as the introduction of probing instruments can have

substantial effects on these values and render signal propagation from probe to amplifier impossible due to improper load matching. Resistance of tissues can reach as high as 1 to 10 MΩ, and increases in an inverse proportion to the frequency of the signal they propagate [11]. To minimize this effect, the use of silver/silver chloride electrodes as well as the use of high current sensitivity operational amplifiers are used in the design and experimentation. Next, the amplifier must be designed with downsizing in mind. For testing within this thesis, larger components will be used for ease of construction, however custom printed circuit boards, pictured in chapter 1, are designed to maintain a small dimension. Outputs of the amplifier show ideal gain characteristics, amplifying mV signals up to a practical gain of 600x. Variable gain is controlled by a potentiometer for adjustment of amplification level, as well as a DC voltage offset also controlled by potentiometer to keep all measured voltage positive. All these factors mentioned account for all the criteria of a proper biosignal amplifier, including high SNR, proper impedance response, and the potential for even further downsizing in later developments of biomedical device implementation.

Properties of Optical Materials

Optical fiber presents many advantages thus far not fully explored within the realm of biomedical device design. Primarily, optical fiber is designed to transmit information in the form of optical pulses, similar to the electrical impulse trains utilized in neuronal communication [9]. Secondly, optical fiber is most often designed with non-reactive materials, coatings, or a combination of both. These materials include polymers of silicon, germanium, gallium, or indium, or in some cases can be composed entirely of a single element like silicon. The basis of optical communication within an optical fiber relies on properties of internal reflection within the fiber, preserving the signal as it travels through the medium at extremely high speeds. Insulation from noise is another factor to be considered when using optical fiber, as thus far no biological processes within human tissue communications have been observed to rely on the same near infrared wavelengths used by those in optical fiber. This implies then that any use of optical fiber devices for artificial implanted biosignal measurement devices will pose no risk of interfering with naturally occurring signals therein. These factors combined suggest that the use of this fiber for neuronal signal transduction within implanted devices should not be overlooked.

For the purposes of this experiment, conversion to optical signal will be achieved using the OD110LDS near infrared optical diode. A signal will be passed through the diode and the light passed through an optical tube assembly and received by a silicon detector designed to receive near infrared light. The fundamental

mechanism of optical communication is modulation of light through a waveguide. This modulation signal is passed through a diode used to change the optical intensity based on the current passing through the diode. These changes in intensity can be deconverted by optical intensity sensors to then acquire the originally measured waveform. Fig. 1.1 details the optical tube assembly with projected light paths. From left to right, the construction consists of the optical diode, a 50mm extension tube, a 50mm focal distance lens, another 50mm extension tube, and finally the silicon photodetector to receive the focused light.

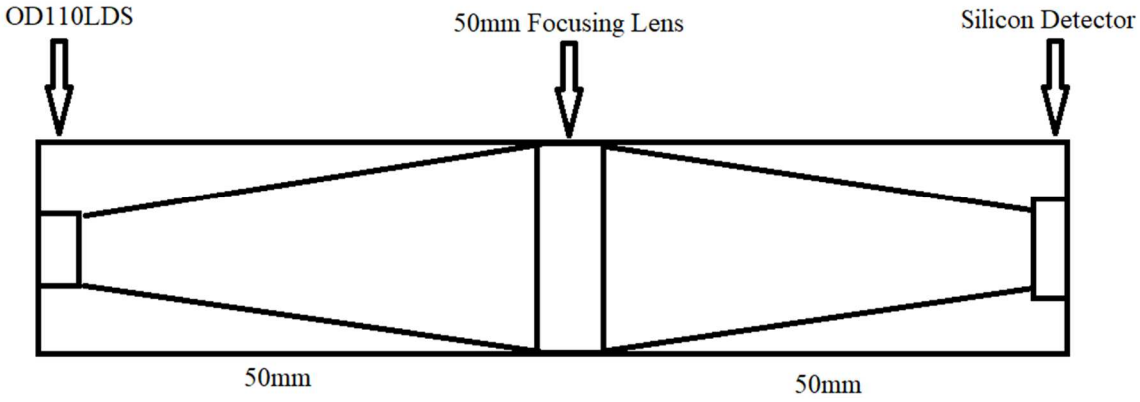

Fig. 1.1: Diagram of Optical Tube Assembly

Experimental Outline

The experiments performed in this thesis will seek to prove two things. Firstly, that the design of this bioamplifier is capable of acquiring bioelectric measurements without substantial signal degradation or loss. Secondly, that these signals are capable of being passed through an optical conversion process and received as a light modulated signal while preserving both waveform geometry and frequency data. Voltage loss along the optical medium is not considered in the case of the optical converter, as this signal can be amplified if these two factors are preserved.

The tests will begin by first calibrating the device to understand both real-world gain behavior and settling times, factors both critical to the proper reception of tissue signal measurement. To this end, the amplifier will have the reference electrode grounded, and the input signal being supplied with various values provided from a Keysight EDU33212A Waveform Generator. The amplifier will also be powered to its proper rail voltage of +/-16V with the use of the Keysight EDU36311A Programmable DC Power Supply. The function generator will have outputs measured at various gain levels, as well as various input impedance to determine the gain curves, settling time, and current sensitivity of the device.

Once these values have been taken, a silver/silver chloride electrode will be constructed by placing a silver wire anode and platinum wire cathode in a 0.1 molar concentration of hydrochloric acid, and supplied with 10mA of current over the course of 1 minute [12]. This electrode will then be placed used to measure both mouse phrenic nerve and cardiac tissue. These outputs will be recorded by the

use of a coaxial cable input to the Analog to Digital Converter (Analog Discovery 2) connected to the Waveforms software for data measurement.

When tissue measurements have been successfully acquired, the data will be recorded and imported to a waveform generator. These recordings, as well as similar waveforms will be generated by the function generator into the optical test bed. The optical conversion will be achieved with the use of the OD110LDS near infrared optical diode and passed through a hollow optical tube assembly described earlier in this chapter in figure 1.2. An Edmund Optics TO-5 silicon photodetector is then used to acquire the measurements of the focused light which are recorded similarly to the tissue outputs. These results will then be compared to determine the capability of the device both as a standalone bioamplifier, as well as a device capable of driving the types of voltages needed for optical conversion.

Hypothesis

The hypothesis presented in this thesis states that a small, lower power device can be designed to amplify bioelectric extracellular signal events to levels capable of clearly being carried along an optical medium. This device would be capable of effectively transferring the information of that signal without substantial loss or signal degradation. This will be done by designing a downsized bioamplifier and recording the outputs. Signals similar to these amplified signals will then be passed through an optical bridge and compared to the originally measured signal from the amplifier results.

Aims

There are a few key aims outlined in this thesis, all of which are for the purpose of proving the concepts of the necessary design methods for implantable device purposes. Firstly and most importantly, the device described here is meant to capture measured electrical signals gathered from tissue samples to a level that can be accurately conveyed along an optical medium. Accurate, in this case, implies the preservation of the original waveform within temporal accuracy, however the nature of optical conversion means that the measured voltages after passing the signal through the optical medium will need to be re-amplified in order to reflect the actual measured potentials at the probe site. For example, a signal measured between -50mV and +50mV may be converted to a signal that measures between 2V and 3V after an optical medium, so accuracy is described here as proper preservation of frequency and waveform information of the amplified signal, as the measured geometry of the waveform including spikes, troughs, peaks etc. should not be affected.

Secondly, this project aims to substantially downsize the physical dimensions of devices commonly used to acquire such waveforms from tissue samples. Products like the Axopatch 200B line of bioamplifiers have dimensions of 3.5 x19 x12.5 inches, making them impossible to implement for implantable devices. By limiting the number of features on the amplifier, as well as utilizing lower power components, the size of such a device can be substantially reduced while performing similar functions.

Lastly, few devices available to the public utilize an optical medium for the transference of bioelectrical signaling. This thesis seeks to prove that these acquired signals can be effectively converted after the use of such a downsized biosignal amplifier device without sacrificing signal quality. Optical encoding also has many potential advantages outlined in the abstract, including small size and resistance to bodily interference.

Results

To address the goals outlined above, a device was created for this thesis consisting of a low power bioamplifier and optical encoding system. This device is capable of effectively amplifying tissue measurements to the levels necessary to drive an optical diode capable of modulating optical intensity for the purpose of encoding the biosignal information. This signal will then be deconverted back to electrical signal with the use of a component capable of demodulating the changes in optical intensity of the signal back to that of a strictly electrical waveform. This device is capable of running on a total supply of approximately +/- 16 volts, and has a total dimension of 2.5 inches by 4 inches. Both the amplifier and optical modulation circuits proved capable of the task of capturing and encoding bioelectric signals. Detailed results of this device are outlined in the results section of chapter 4.

Conclusion

The device outlined and tested in this thesis has enormous implications for future designs of biomedical devices meant to act on regions of damaged or diseased nerves. The proper transduction of bioelectric impulse signals at small scales can be utilized in the development of optical nerve bridges and other similar devices for treating spinal cord injuries, degenerative nerve diseases, and eventually even prosthetics that could be controlled by neural impulse signals interfaced via optical devices. This technology could also be utilized in neuromodulation devices meant to help regulate action potential activity in many areas of the body.

References

[1] Åke Bernhard Vallbo, “Microneurography: how it started and how it works,” *Journal of Neurophysiology,* Vol. 120, Iss. 3, pp. 1415-1427, 2018.

[2] T. Mano et al, “Microneurography as a tool in clinical neurophysiology to investigate peripheral neural traffic in humans”, Clinical Neurophysiology, Vol. 117, Iss. 11, 2006.

[3] Lawrence Stark, Jose Negrete-Martinze, Guillermina Yankelevich N., George Theodoridis, “Experiments on Information coding in nerve impulse trains”, Mathematical Biosciences, Vol. 4, pp. 3–4, 1969

[4] Abraira, Victoria E, and David D Ginty. “The sensory neurons of touch,” Neuron vol. 79, Iss. 4: pp 618-639, July 2013.

[5] D.M. Wilson, W.J. Davis, “Nerve Impulse Patterns And Reflex Control in the Motor System of The Crayfish Claw,” *Journal of Experimental Biology* Vol. 1, Iss. 43, pp. 193–210. October 1965.

[6] A. Mark Evans, Christopher N. Wyatt, Nicholas P. Kinnear, Jill H. Clark, Elisa A. Blanco, “Pyridine nucleotides and calcium signaling in arterial smooth muscle: From cell physiology to pharmacology,” *Pharmacology & Therapeutics* Vol. 107, Iss. 3, pp. 286-313, March, 2005.

[7] Rudolf R, Khan MM, Witzemann V, “Motor Endplate—Anatomical, Functional, and Molecular Concepts in the Historical Perspective.” *Cells,* Vol. 8, Iss. 5, pp.387, 2019.

[8] Pujitha Weerakoon, Eugenio Culurciello, Youshan Yang, Joseph Santos-Sacchi, Peter J. Kindlmann, Fred J. Sigworth, “Patch-clamp amplifiers on a chip,” Journal of Neuroscience Methods, Vol. 192, Iss. 2, pp. 187-192, 2010.

[9] Kaiser, Gerd, Optical Fiber Communication 4th Edition, New York: McGraw Hill Publications, 2011.

[10] Sontheimer H., Ransom C.B., “Whole-Cell Patch-Clamp Recordings. In: Walz W., Boulton A.A., Baker G.B. (eds) Patch-Clamp Analysis”. *Neuromethods*, Vol 35. 2002.

[11] E T McAdams, J Jossinet, “Tissue impedance: a historical overview,” Physiol. Meas. Vol. 16, Iss. 1, 1995.

[12] Gaston A. East, M. A. del Valle, “Easy-to-Make Ag/AgCl Reference Electrode,” *Journal of Chemical Education,* Vol. 77, Iss. 1, pp.97, 2000.

Chapter 2

Simulations and Calculations

Before a physical test apparatus can be built, simulations must be done of each component to determine proper parameters needed for an application like this. The most important parameters to consider when designing an amplifier for the purpose of this context are as follows; extremely low noise, variable linear gain, proper filtration, and tunability in relation to the resting membrane potential of the cells being measured as well as how these values change. As stated previously, the resting membrane voltage of a typical neuron is around -70 mV, with a peak action potential voltage of around 35 mV. As such, the amplifier will be designed to amplify this voltage range. It will also include a -70mV tunable DC offset on the positive terminal of the main amplifying unit within the circuit. This is to ensure that the entire acquired signal is amplified above 0V. This amplifier design will be based largely off of the paper “Patch Clamp Amplifier on a Chip” by Pujitha et al [8]. There will be several key differences, primarily relating to changes in the structure of filtration circuits and addition of further noise reducing passive elements in place of onboard DACs like those found in the paper.

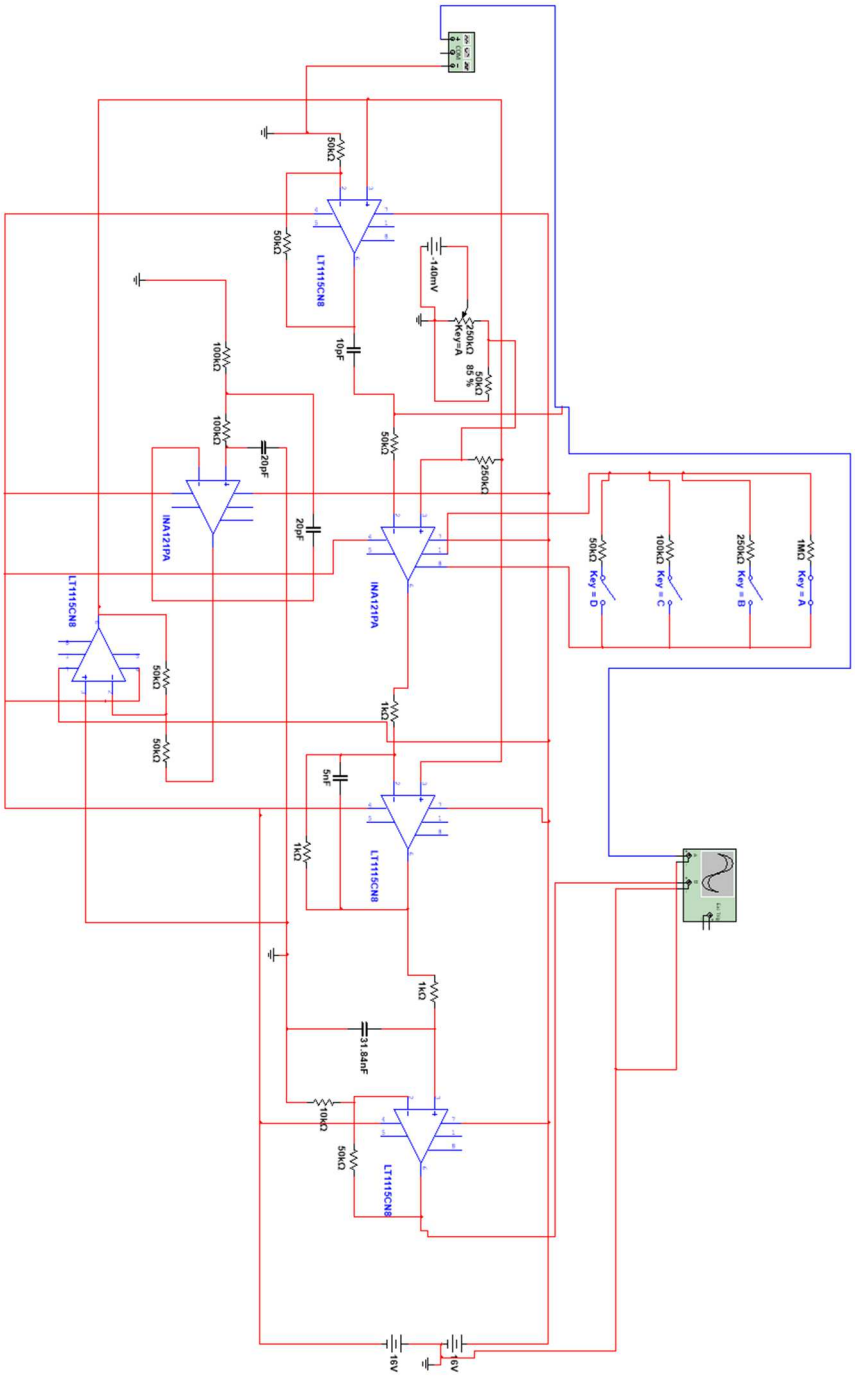

Fig. 2.1: Multisim Schematic of Biosignal Amplifier with Function Generator and Oscilloscope

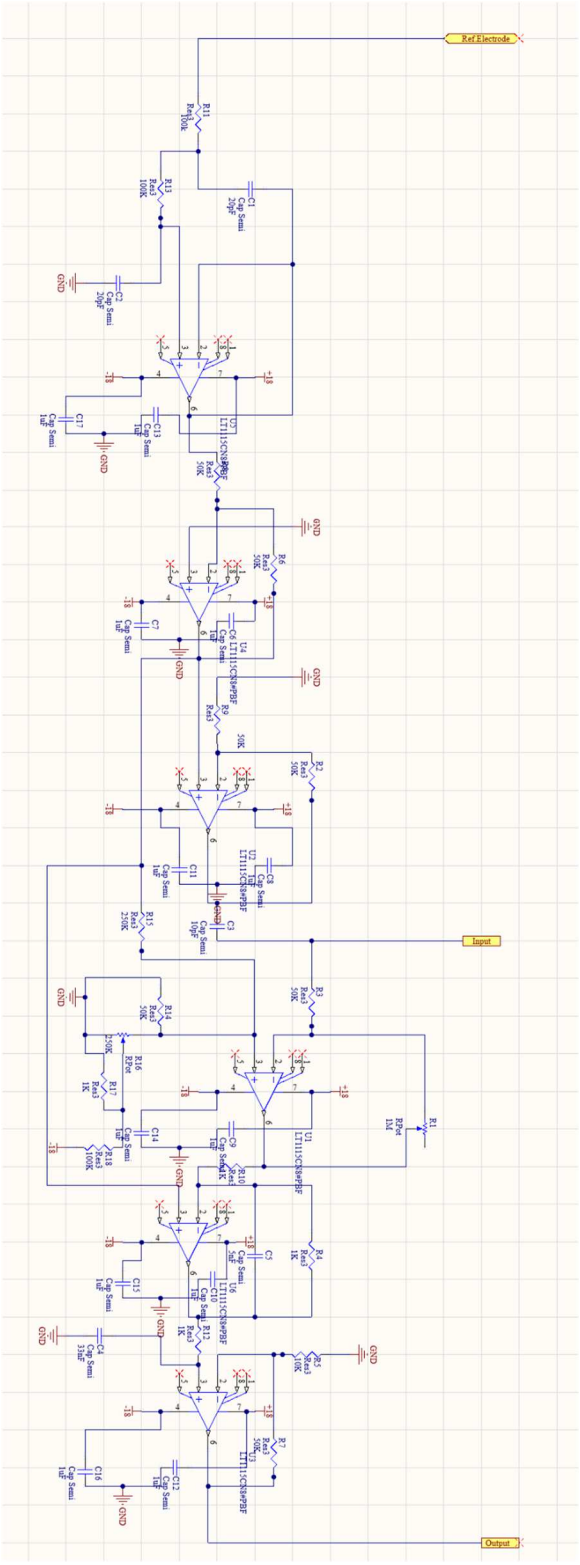

Fig. 2.2: Schematic of Biosignal Amplifier in Altium Layout

Fig. 2.1 is a complete diagram of the circuit designed for this application. It contains the components necessary for a reference electrode input buffer, a variable gain amplifier, DC offset at the probe input, and a 5 KHz filter with gain before the output. When used at the maximum gain setting, this amplifier boasts an approximate gain of 50dB, making the output signal powerful enough to drive the optical diode operating between 1.5 and 2V forward voltage. The introduction of the reference electrode in combination with the manual DC offset to the input electrode ensures that the bioelectric signals of the cell will be properly isolated and amplified. All simulations done below are done by grounding the reference electrode and connecting the virtual function generator directly to the input stage of the amplifier, as shown in figure 2.1. Outputs are recorded in the virtual oscilloscope, with red signals indicating the output and blue signals indicating the input. Fig. 2.2 details the outline of the circuit after testing that is ported to Altium for fabrication of a custom circuit board and is identical in function.

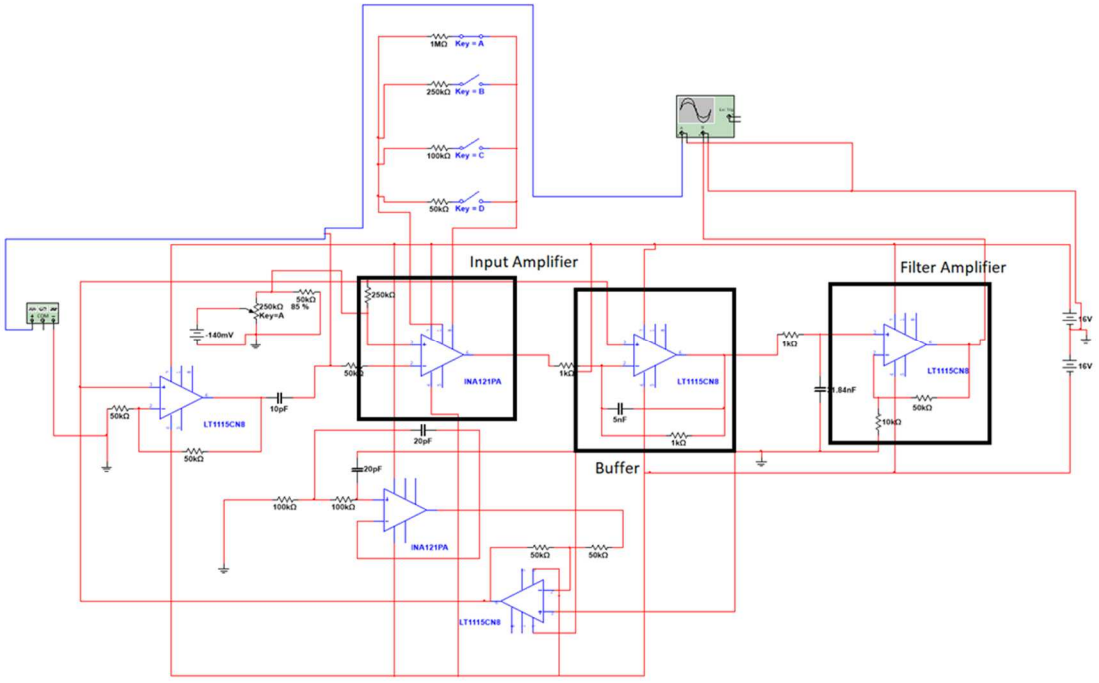

Fig. 2.3: Highlight of the Input Electrode

Fig. 2.3 highlights the particular elements of the input electrode. It consists of an INA121PA input operational amplifier with two inputs. The tissue probe connects to the input while the other connects to the output of the reference electrode to combine the resultant signal into one that isolates the desired signal from the noise of the environment. This stage also has an amplifier gain controlled by a single resistor placed between pins 1 and 8. The equation for the gain of this circuit is shown below:

$$\square\square\square\square = 1 + 50\square/\square$$

Wherein R is the resistor placed between these pins. In practice, this gain is controlled by a 1 MΩ potentiometer, however for clarity in simulated results a stack of switchable resistors is used. The output of this amplifier is then passed to an

inverting buffer with an overshoot corrective capacitor, the details of which are further explored below. The final stage of this section is a 5 KHz low pass filter with a linear gain of 6, allowing for a final stage of filtration and amplification of the desired signal.

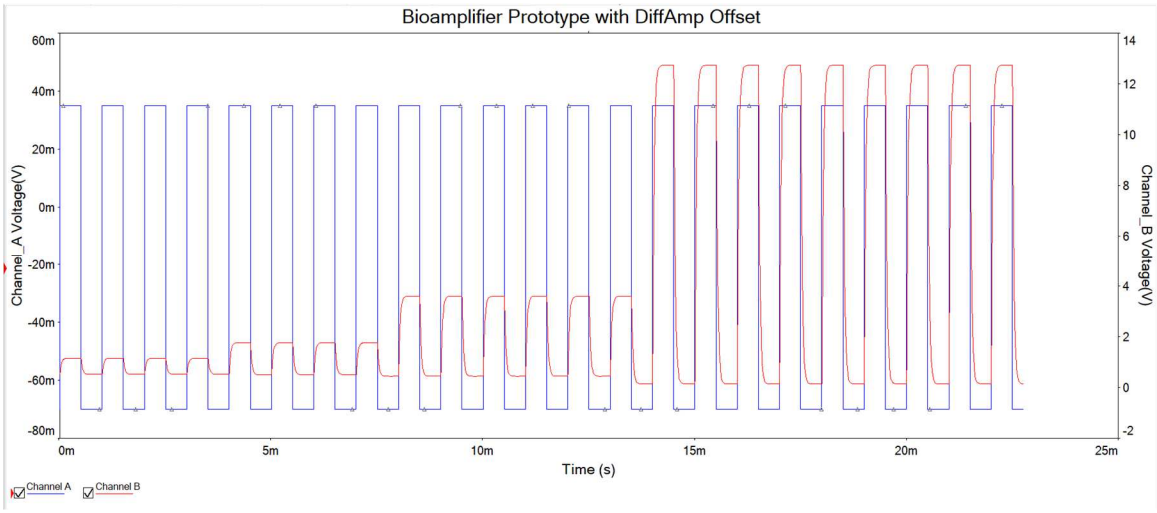

Fig. 2.4: Input (Channel A, Blue) and Output (Channel B, Red) as Linear Gain is Increased

Fig. 2.4 demonstrates the change in output as gain is increased. This is done without the presence of the DC offset for this example. Each change in wave amplitude of the output represents an increase in the linear gain of the primary amplifier by increasing the variable resistance of the feedback potentiometer. In order, the linear gain of each step begins with unity, then increases to two, then five, and lastly a linear gain of twenty. Each signal is amplified by a linear factor of six by the non-inverting low pass filter at the last stage of the circuit, creating a maximum linear gain of 120, or about 41dB.

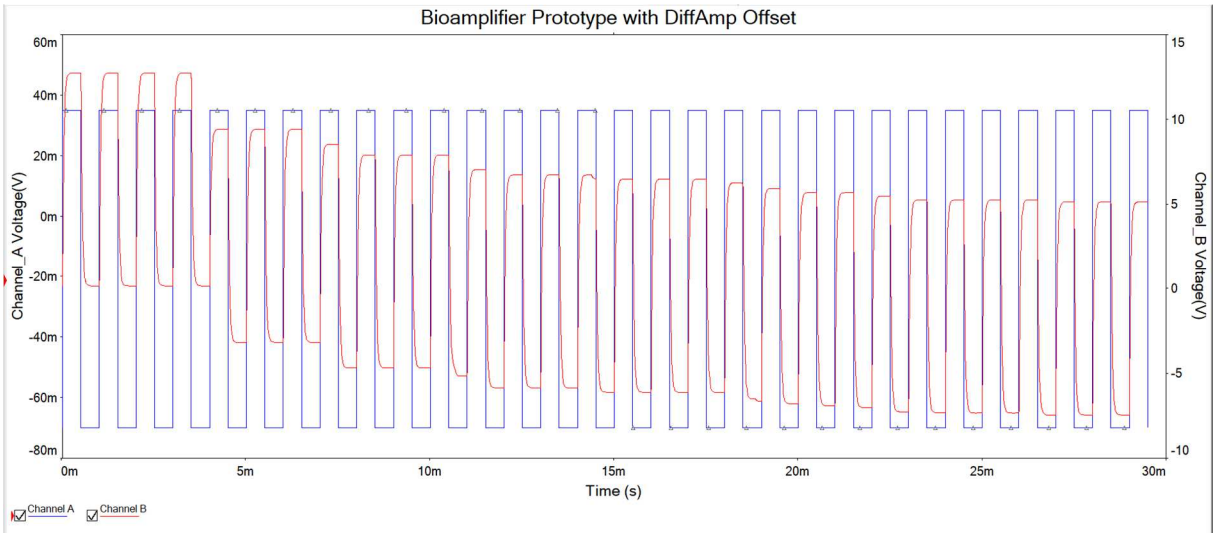

Fig. 2.5: Change in Output as DC Value is Adjusted

Fig. 2.5 demonstrates the effectiveness of the DC offset fed into the positive terminal of the primary amplifier. This offset is meant to provide a differential non-zero voltage by which the amplifier has a reference of amplification. As seen above, a simulated input pulse with a resting potential of -70mV can be raised above zero by the differential offset. This has the effect of taking any input signal to be amplified to strictly positive voltage, allowing for ready conversion in the optical driver. As the DC offset is increased from -70 mV to zero, the DC offset of the signal decreases to include amplification of the negative signal. While this is not inherently problematic for the function of the circuit or the device as a whole, it allows for a greater level of control when trying to adjust for resting potential during measurements.

It should be noted that there are other methods commonly used to ensure that the amplified signal is only that of the membrane voltage change above resting, the

most common of which is to use a powered probe of the same voltage as resting potential. This ensures that the effective voltage at the site where the probe meets the cell is zero and that any changes in membrane voltage are fed directly to the amplifier circuit. In the case of implantable devices however, powered probes are not ideal for two primary reasons. Firstly, powered probes would require that an entirely separate tuning system be built from another power source, or possibly even diverted from a main power source. This would most likely require the construction of additional buffers and control circuitry, inflating both cost and space requirements. Secondly, powered probes have the potential to change input measurements by introducing noise into the system, or affecting the resting potential of the membrane being measured if the power delivered to the probe is not exactly matched to the membrane voltage. For these reasons, a passive probe was chosen and a manual DC offset was added to the circuit design, as well as to introduce the opportunity of a technician to independently tune the offset voltage on an individual basis.

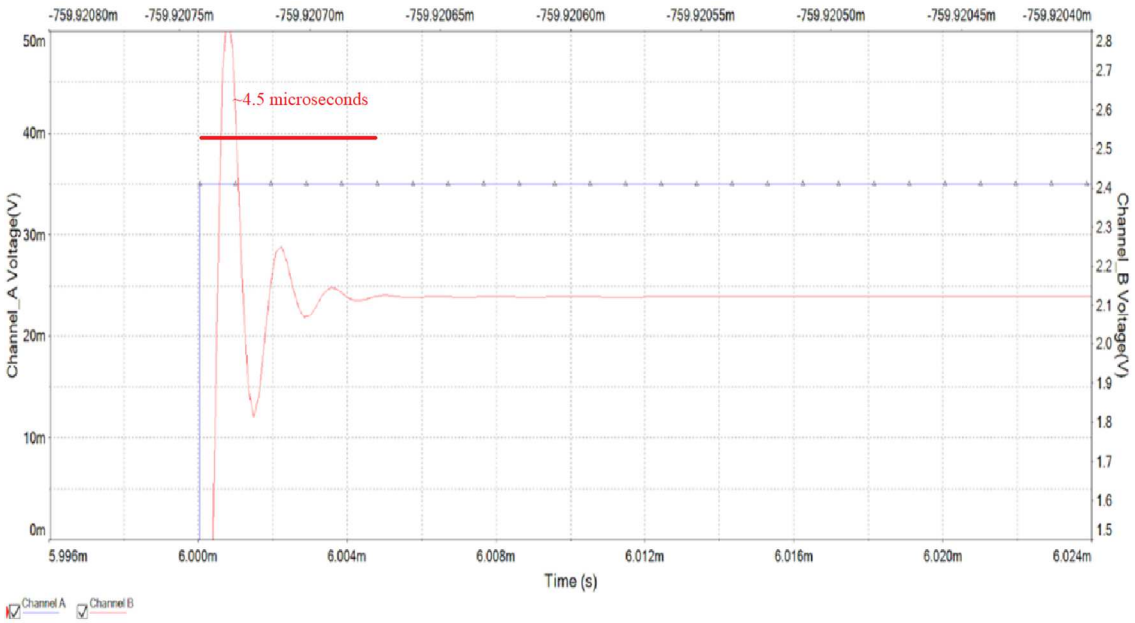

Fig. 2.6: Overshoot of Amplified Signal

Initial testing of the circuit revealed that immediately after the primary amplifier and amplifier buffer, the signal was prone to overshoot and an unstable transient response at each rising edge of the impulse train. This creates a substantial problem for the quality of the signal being amplified. While the 5KHz filter that immediately follows this buffer is capable of reducing this noise, it is ideal to eliminate any potential noise at the source rather than rely on this filter meant to eliminate noise from the environment. To this end, a capacitor is added to the feedback loop of the buffer shown in figure 2.7. This is meant to change the loop gain behavior of the buffer in a manner that increases stability of the signal being amplified. While this could be added to the primary amplifier, this would change the feedback loop of the amplifier in a way that could affect its gain profile.

A typical differential amplifier will have a loop gain equation of

$$A\beta = \frac{aR_G}{R_F + R_G}$$

in which A describes the loop gain, ‘a’ is the open-loop gain, Rg is the input resistance and Rf is the feedback resistance. By adding a feedback capacitor to the closed feedback loop, the equation is changed to

$$A\beta = \frac{aR_G}{R_F + R_G} \times \frac{R_F C_F + 1}{R_F \left\| R_G \left(C_F + C_G \right) + 1 \right.}$$

in which C_F is the feedback capacitor, and C_G is an input capacitor. The equation here details a scenario in which a positive phase shift occurs in the loop-gain plot of the circuit, increasing the stability [13]. This occurs because the effective filtration of the circuit is now below the oscillation frequency of the overshoot, preventing it from passing through the buffer. This event only occurs if two criteria are met. Firstly, the closed-loop gain must be greater than or equal to one, and secondly C_F must be greater than C_G [13]. Considering that there is no input capacitance and that we have a unity gain buffer, both of these criteria are met. Through testing, the smallest functional capacitor was added to the buffer to achieve overshoot correction without creating unnecessary delay in the transient response time of the buffer, a value between 1 and 5 nanofarad effectively corrects the overshoot.

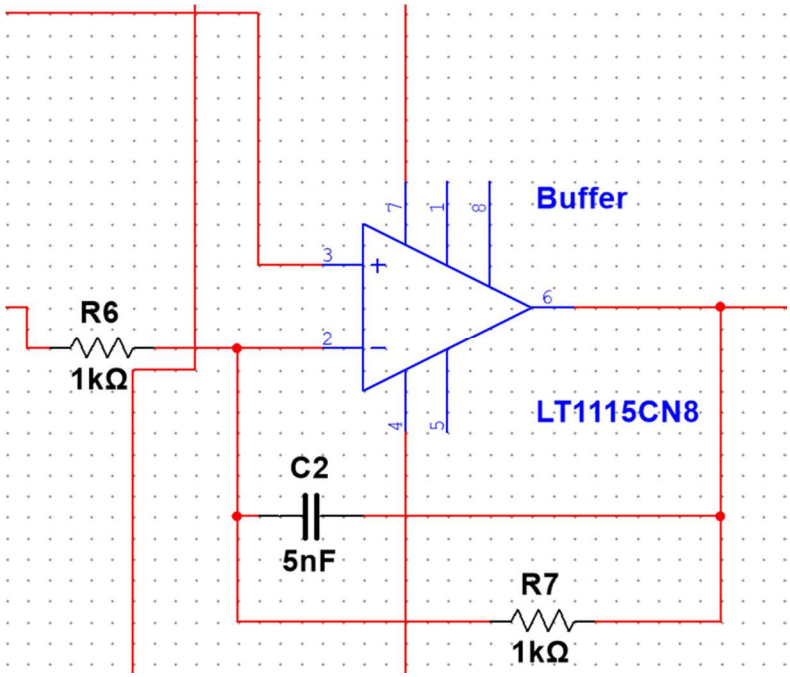

Fig. 2.7: Unity Gain Buffer with Added Feedback Capacitor

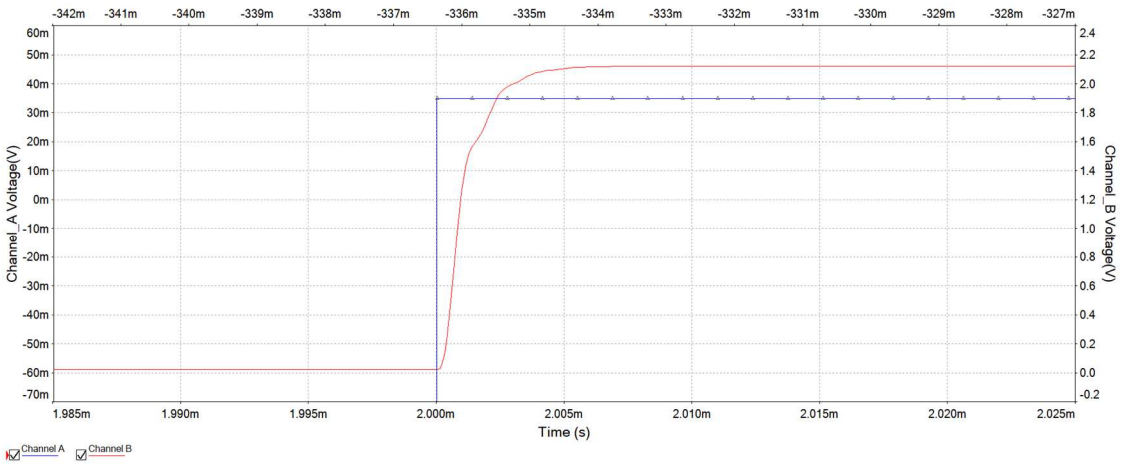

Fig. 2.8: Overshoot Correction as a result of added Capacitor

As seen in Fig. 2.7, the placement of this capacitor successfully corrects the overshoot without creating an additional delay between transient and steady state response of the amplifier, a period of approximately 4 μS which is well within acceptable tolerance for this application.

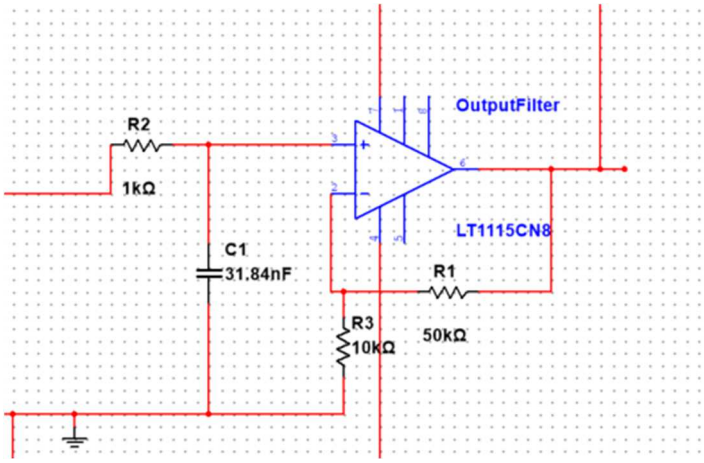

Fig. 2.9: Non-Inverting Low Pass Filter with Linear Gain

Now that stability has been demonstrated in the amplified signal, another critical element of bioamplifier design must be addressed. Proper filtration of biosignals is important to prevent unwanted noise from entering the optical driver. Initially, a bandpass filter was considered but ultimately deemed not ideal as neuronal impulse trains typically occur between 100-300 Hz [2]. To this end, a non-inverting 5 KHz low-pass filter is implemented here. The 5 KHz frequency is common in bioamplifier design, as signals detected above this frequency are almost always attributed to noise, given that the refractory period of most cellular signaling prevents signals from approaching this frequency range. A noninverting design was used to prevent the final output signal from becoming inverted, allowing for consistency between input and output. Lastly, a final amplification stage is added to this circuit to ensure that only the proper frequency signals are amplified to the output of this amplifier and passed into the optical component.

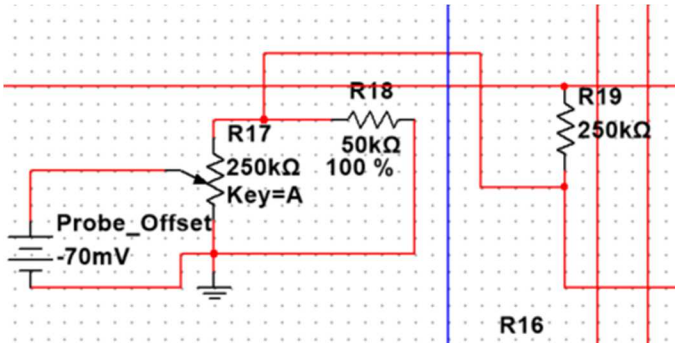

Fig. 2.10: Variable Voltage Divided Differential Probe Bias

As mentioned previously in this section, a probe bias is required to ensure that any signal being amplified is a result of the increased voltage above the resting potential of the membrane being measured. Having a direct -70 mV offset voltage difference on the probe is not ideal however, as this could lead to a discrepancy between actual measured membrane voltage values and the offset. To this end, a voltage divided offset knob has been designed as seen in fig. 6. This probe divides a small, negative mV range source that increases to a 0V offset as the potentiometer used is increased in value. In the event that resting membrane potential is slightly above the typically expected value, this potentiometer grants the ability to fine tune to the actual resting membrane potential at the measurement site. Final designs of testing parameters have this maximum offset value at approximately -180mV to ensure a wide range of tissue type may be measured by this configuration.

A large resistor is placed in between the input of the probe and the output of the capacitance buffer circuit to ensure that this DC offset does not apply to any other areas of the circuit, and instead only acts on the positive terminal of the primary

amplifier. Without this, the offset voltage could affect all of the other circuits that connect to the output of the reference electrode buffer in the same way as the amplifier and create substantial instability.

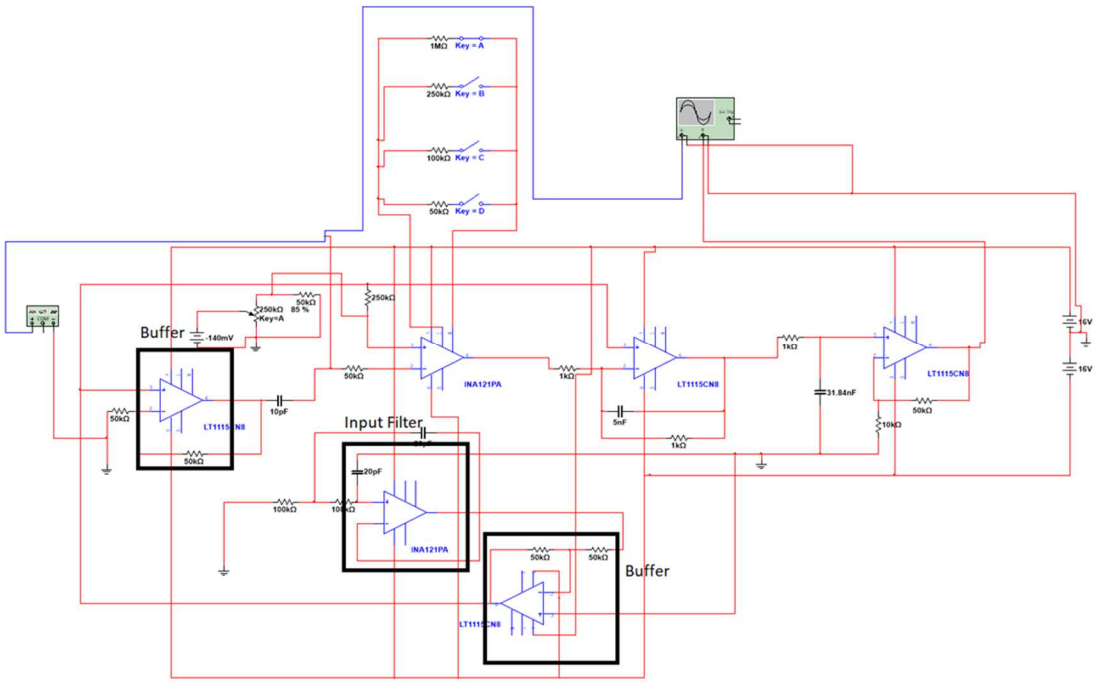

Fig. 2.11: Two Pole Reference Electrode Filter with Unity Gain buffer

Fig. 2.11 outlines the reference electrode with input buffer. It consists of a two pole input filter, a unity gain inverting buffer, and a unity gain non-inverting buffer. The filter is inverting in this case, and as such the reference value must be inverted to ensure that the signal being amplified is differential to the environment. The remaining non-inverting buffer is meant to act as a preventive, keeping the signal

from the input electrode from flowing backward through the reference electrode circuitry. This reference electrode output is also passed to the non-inverting terminal of the main amplifier and the buffer immediately following to provide correct differential offset in reference to the environment of the measurement probe.

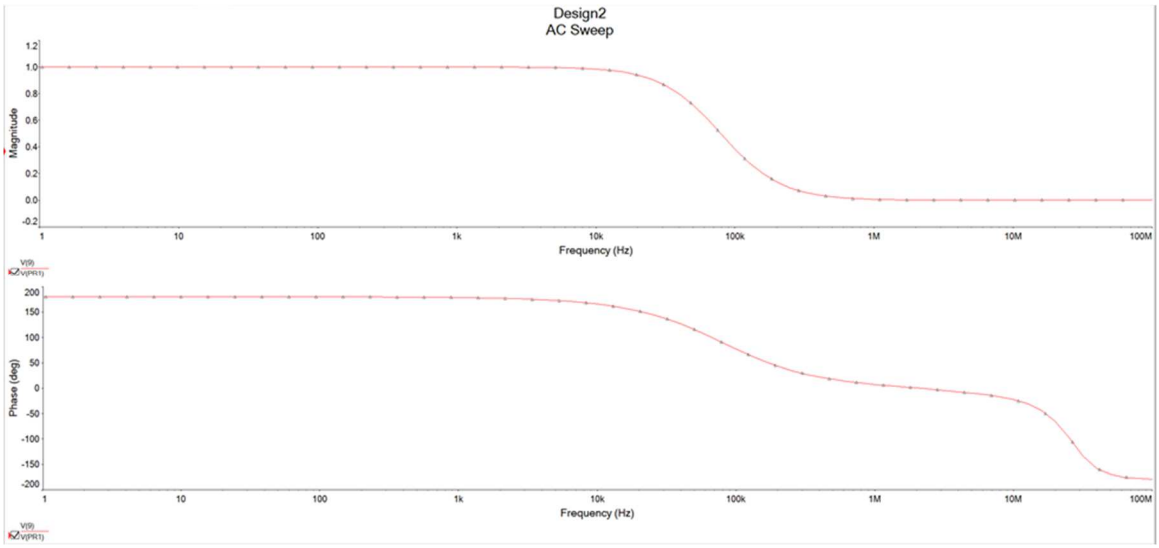

Fig. 2.12: AC Sweep Analysis of Reference Electrode

Fig. 2.12 details the AC response of the reference electrode input buffer, demonstrating a cutoff frequency of approximately 80KHz. This value is intentionally higher than predicted measurement values to account for voltage fluctuations in the probe environment, while not allowing substantially higher frequencies associated with environmental noise to pass through and disrupt amplification behaviors.

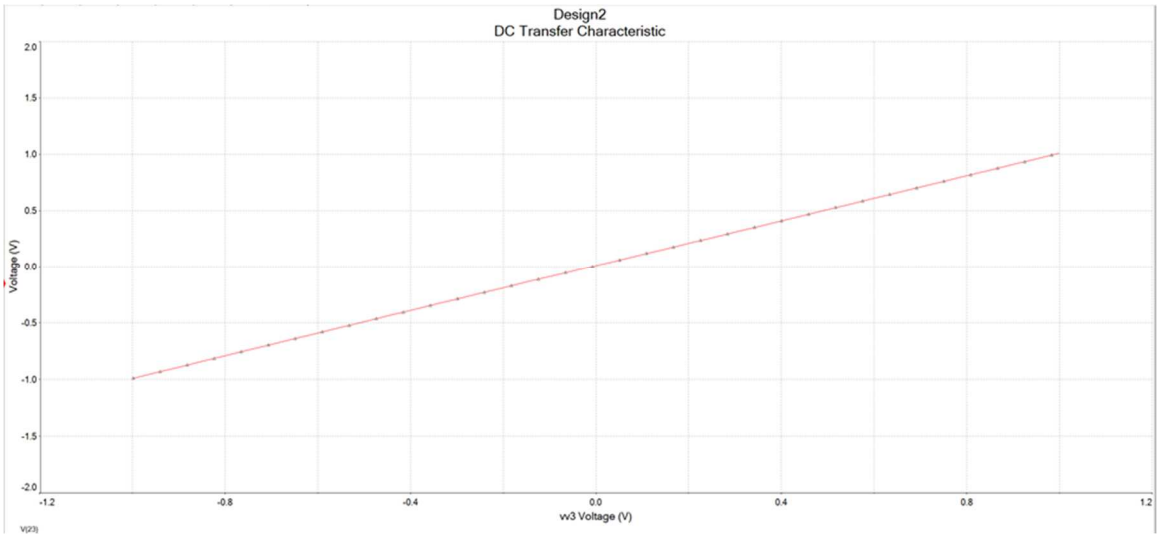

Fig. 2.13: DC Sweep Analysis of Reference Electrode

Fig. 2.13 demonstrates that there is a unity gain within the reference electrode buffer, ensuring that no additional signal is introduced to the system by the presence of this circuit. Both the DC and AC analysis associated with this region of the circuit include the two-pole filter and inverting buffer to best represent how the signal being continued to the rest of the circuit will behave.

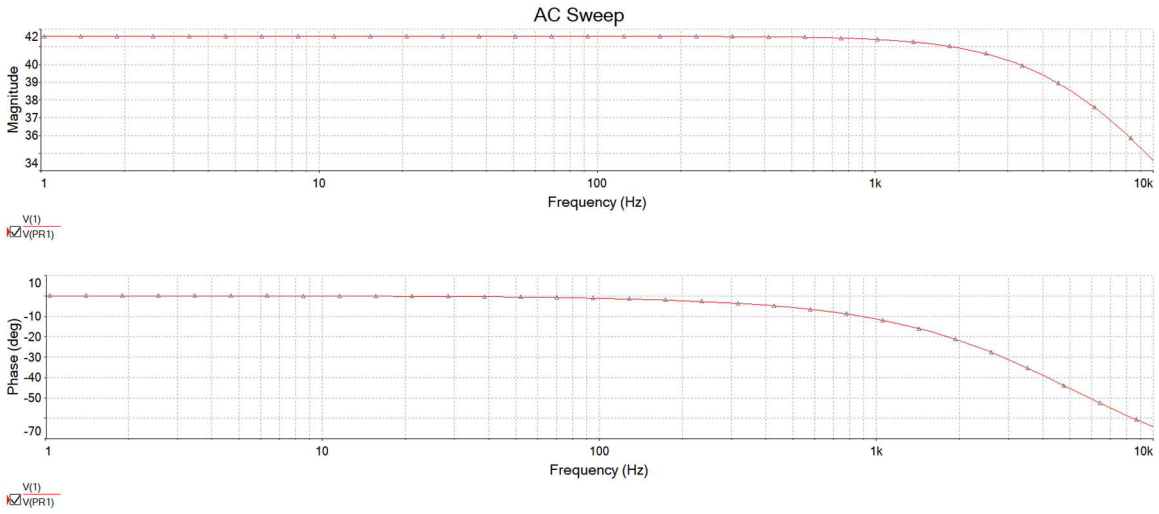

Fig. 2.14: AC Sweep Analysis of Amplifier

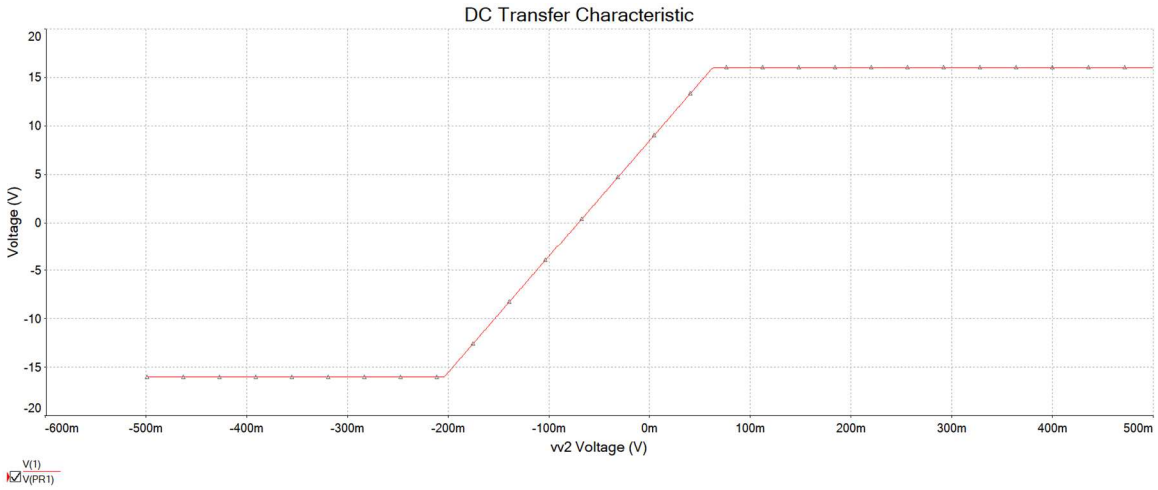

Fig. 2.15: DC Sweep Analysis at Maximum Gain

Figures 2.14 and 2.15 detail the AC and DC sweep analysis of the entire system when the reference electrode is grounded and all operational amplifiers are supplied with both positive and negative 15 volt sources. As expected, the total AC response of the amplifier has a frequency cutoff of 5 KHz and DC cutoffs at the supply voltages. Within the functional region of DC output values though, maximum gain is used for the analysis and demonstrates the expected decibel gain of the system to be a continuous, linear response.

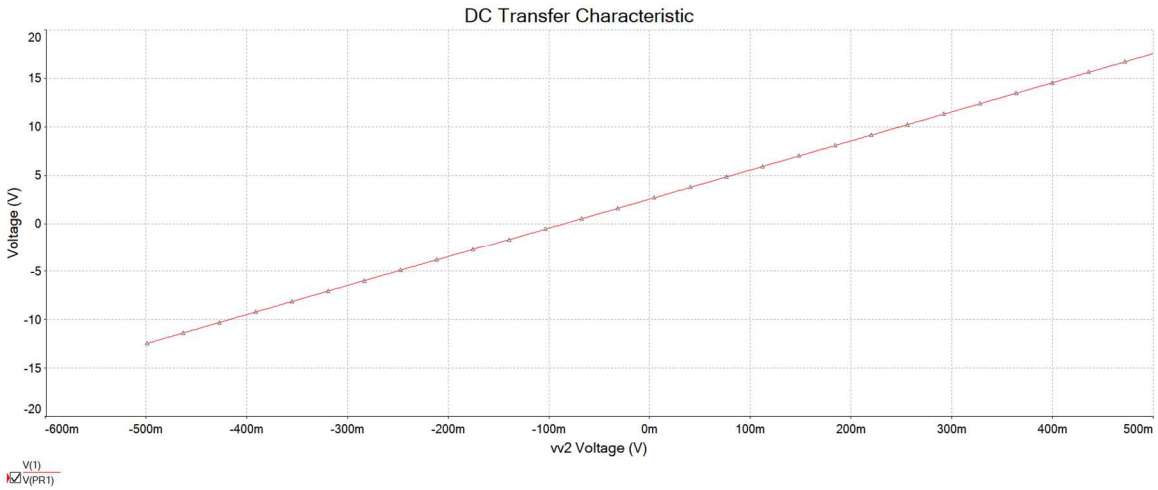

Fig. 2.16: DC Sweep Analysis at Linear Gain of 6

When simulating with a linear gain of 6, the clipping caused by the operational amplifier is not present and further demonstrates a continuous linear response of the system.

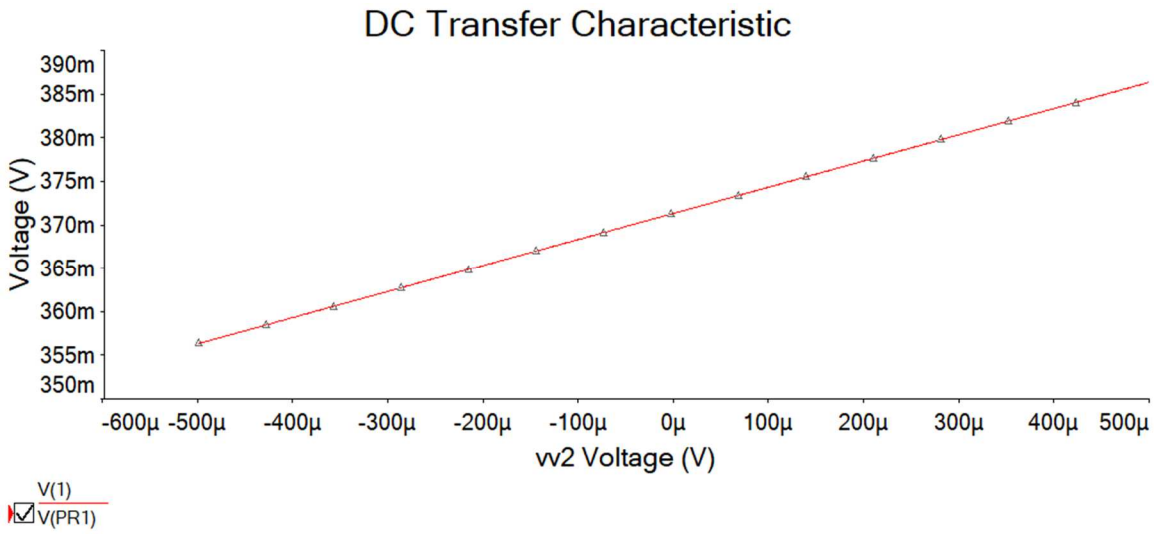

Fig. 2.17: Microvolt simulated response

To demonstrate the full range of capabilities expected of this design, simulations are performed using µV source ranges. The use of the manual DC offset does not affect the linearity of the simulated output, and continues to demonstrate consistency of the signal amplification at such small voltage ranges.

Conclusion

The amplifier proves to preserve linearity and signal quality under many voltage ranges and frequencies. The filters act as designed and prove that the design of the amplifier is sufficient for the use cases outlined in this thesis. With a total maximum gain of 56dB, as well as steps taken to further control distortions of the amplifier such as the feedback capacitor and amplifying filter, the design will be ported to Altium and undergo fabrication into a functional, physical circuit for further testing.

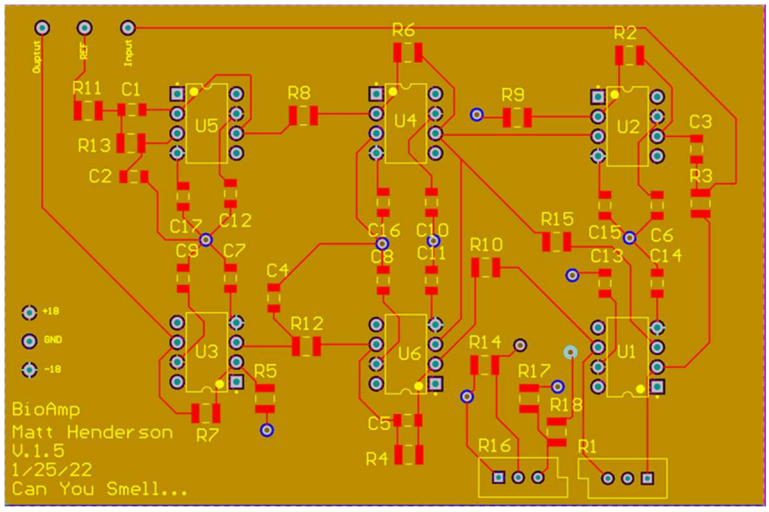

Fig. 2.18: Final Circuit Layout of Altium PCB

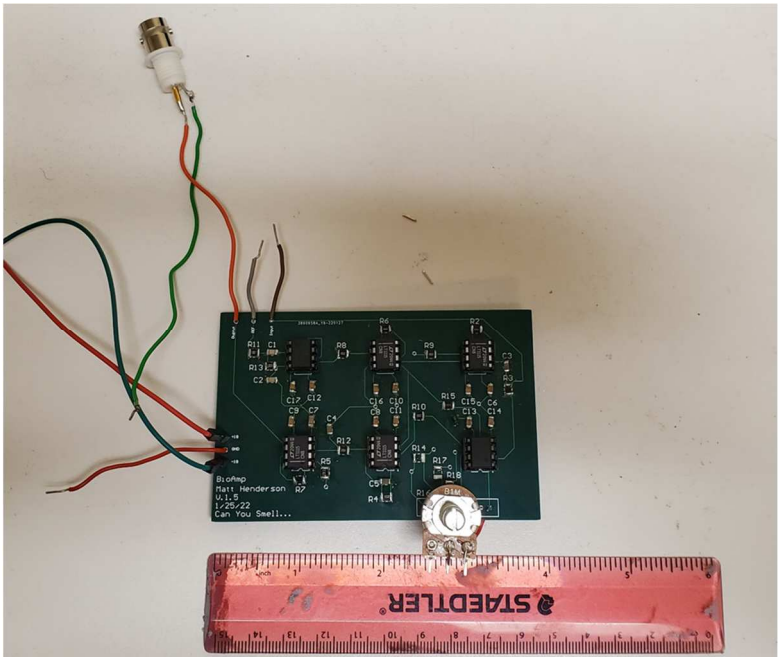

Fig. 2.19: Final Fabrication of Amplifier Circuit, Ruler for Scale

Figures 2.18 and 2.19 are the final Altium layout and fabrication of the board that will be used in all physical testing in this thesis. The physical board is also fitted with a coaxial output and copper wires for attachment to probes later on.

References

[8] Pujitha Weerakoon, Eugenio Culurciello, Youshan Yang, Joseph Santos-Sacchi, Peter J. Kindlmann, Fred J. Sigworth, “Patch-clamp amplifiers on a chip,” Journal of Neuroscience Methods, Volume 192, Issue 2, 2010, Pages 187-192, ISSN 0165-0270, https://doi.org/10.1016/j.jneumeth.2010.06.030

[13] Mancini, R, “Op Amp Stability and Input Capacitance,” Texas Instruments, Dallas, Texas, 2005.

[2] T. Mano et al, “Microneurography as a tool in clinical neurophysiology to investigate peripheral neural traffic in humans”, Clinical Neurophysiology, Vol. 117, Iss. 11, 2006.

Chapter 3

Experimental Procedure

Introduction

The experimental procedure outlined here will document the process used to test the capability of the device, and will have many comparative analyses meant to determine the quality and preservation of tissue measurements at every stage of the amplification and optical conversion. This is to ensure that all stages of the device are functioning properly, as well as to compare the quality of the captured waveform at every stage to determine immediate viability of such a device.

All tests conducted will utilize the same device setup, involving the placement of the device in a grounded faraday cage to eliminate environmental noise, and will make use of a silver/silver chloride electrode (Ag/AgCl). This electrode consists of a thin piece of silver wire coated in silver chloride. The silver uncoated end of this electrode is connected to the amplification device for signal capturing. While some uses of this Ag/AgCl electrode require the addition of a potassium chloride solution acting as a buffer within a glass electrode, the measurement of tissues instead of individual cells does not require such treatment.

Procedure

The first round of testing will determine the loading characteristics of the device. A signal will be passed from the function generator onto the input electrode while the reference electrode is grounded. This will be done by passing directly to the input electrode, as well as with the addition of a 1 MΩ and 10 MΩ resistor carrying the signal to understand how loading factors of settling time and gain are changed in response to this loading. This resistance is meant to mimic the tissue impedance commonly measured by biosignal amplifiers, as well as prove the efficacy of the low current capacity of the amplifier. Once this is achieved, the same faraday cage setup will be utilized when measuring tissues. In each case, tissue preparations will follow a similar procedure outlined in the paper “Electrical Slow Waves in the Mouse Oviduct Are Dependent upon a Calcium Activated Chloride Conductance Encoded by Tmem16a” for it’s similar measurement of tissues. This involves the removal of the necessary tissues in each test after dissection, and their placement onto dishes containing Sylgard elastomer. These tissues will be pinned in place by 120μm diameter tungsten pins to restrict movement of the muscle as a result of stimulation [15]. The reference electrode will be placed into the solution bath of the tissue being measured, and the silver chloride electrode placed into contact with the tissue directly. In the case of the nerve tissue, the electrode will be placed at one end of the nerve, and mechanical stimulation will be applied at the other end about 2cm away.

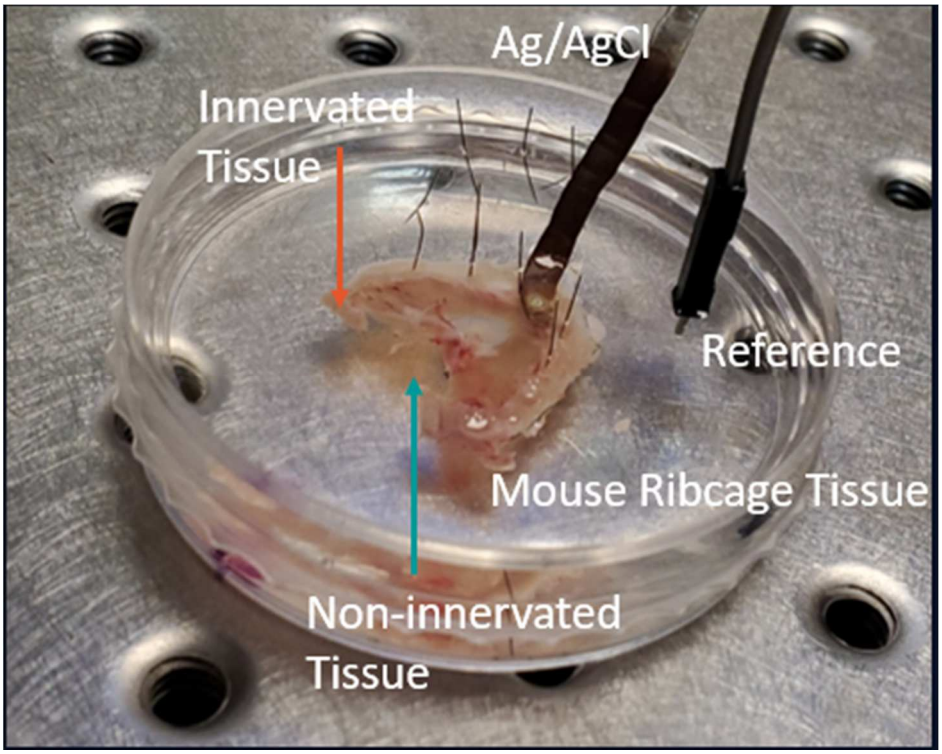

Fig. 3.1: Photograph of Phrenic Nerve Tissue Measurement Setup

In addition to these experiments, mouse cardiac tissue will be measured for action potential activity as well. The electrode will be placed into one of the ventricles of a whole mouse heart, and the heart will be provided with a cycling bath of Krebs solution to encourage electrical activity. This activity will be measured and recorded. To ensure that the recordings are not that of mechanical agitation caused by the beating of this heart, Blebbistatin is used to reduce the movement of the heart. Blebbistatin is a myosin inhibitor, and should act to prevent mechanical activity in the heart while allowing for the electrical activity to remain unaffected. Recordings will be taken after 20 minutes of exposure to this drug.

After the tissue measurements are complete, the waveform generator will be used to create stable signals within the expected output range of the amplifier using data collected from the tissue measurements. These waveforms will then be passed through the optical tube assembly described in chapter 1, and will be recorded using the same setup as the tissue measurements.

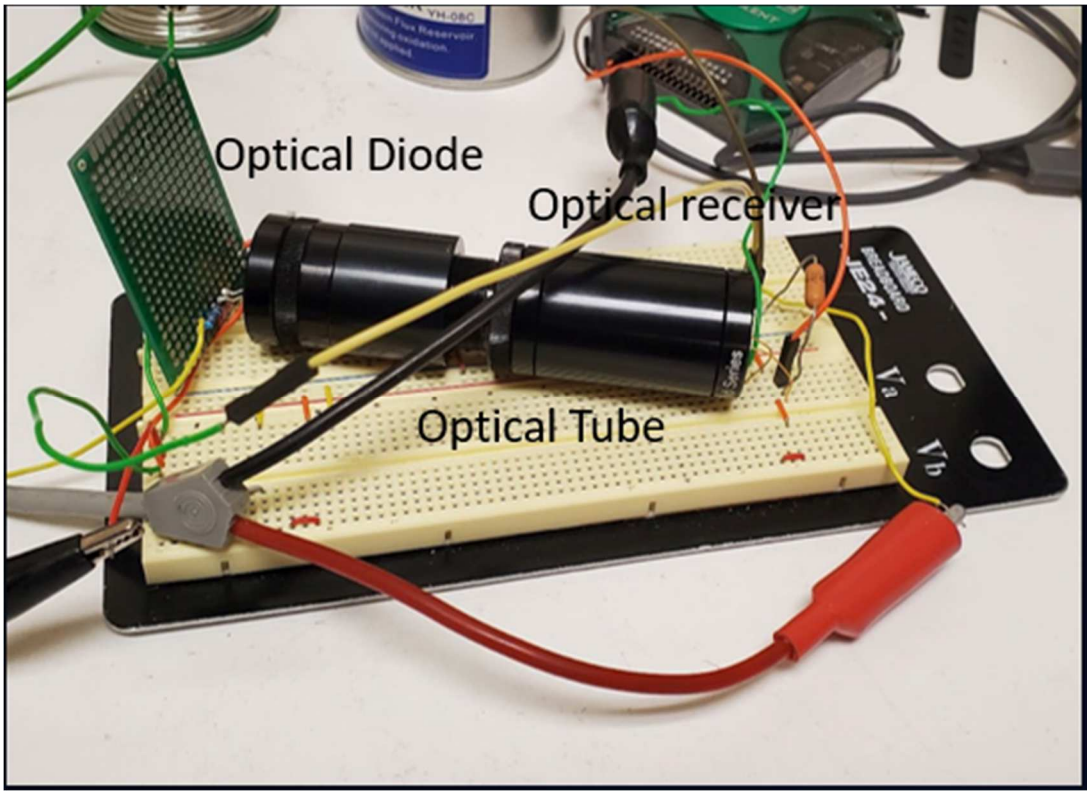

Fig. 3.2: Photograph of Optical Tube Assembly Testing

Comparisons will then be made between the original input waveforms, detailing any signal loss or degradation as a result of the optical conversion process. Results will then be discussed in chapter 4 of this thesis.

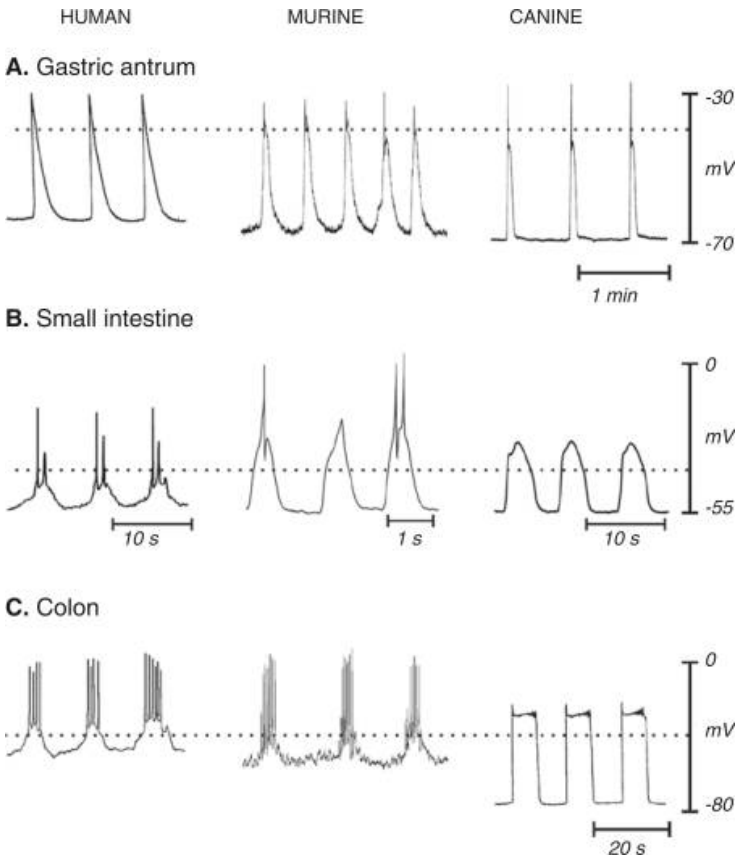

Fig. 3.3: Diagram Detailing different Gastrointestinal Tissue Samples of Human, Murine, and Canine Samples [14]

Figure 3.3 details the recorded outputs of several types of tissue taken from several animal and human sources. In each of these cases, the recorded outputs range approximately within a 100mV peak to peak range. It can be reasonably expected the output measurements of the amplifier designed in this thesis should output similar results, and as such this will be the goal of our tissue recordings.

References

[14] Sanders KM. “Spontaneous Electrical Activity and
Rhythmicity in Gastrointestinal Smooth Muscles”. *Advances in Experimental Medical Biology*, Vol 11, Iss. 24, pp.3-46, 2019.

[15] Dixon, Rose Ellen et al. “Electrical slow waves in the mouse oviduct are dependent upon a calcium activated chloride conductance encoded by Tmem16a.” *Biology of Reproduction,* Vol. 86, Iss. 1 pp. 1-7, January, 2012.

Chapter 4

Results and Discussion

Outputs of Impedance Simulation Test

For the following tests, calibration outputs are gathered based on several criteria. To obtain a sense of how the amplifier would behave differently in simulation versus the environment of a tissue sample, measurements are taken with varying input impedance to determine how it would affect the quality of the signal and amplification. Several Gain curves are produced to determine if the output would remain consistent with the predicted values based on changes to impedance. Additionally, measurements are taken of the average settling time of the signal based on changes to input impedance. In this instance, settling time is determined as the time in which the average value of a changing signal falls within a two percent margin of error from the final value. For each of these tests, a 1 KHz square wave input of 100mV is used, and the variable gain is selected between values of 6x, 10x, 50x, 100x, 300x, and 600x. For settling time calculations, varying input voltages are used at 10mV, 50mV, 100mV, 300mV, 500mV, and 1 Volt. While far higher gain is possible on this device, the practical applications of expanding the gain beyond this are limited by the fact that operational amplifiers used in the amplifier circuit are limited in their maximum/minimum outputs by the rail voltage used to power them. Because of this, 600x was determined to be the highest practical gain for these experiments.

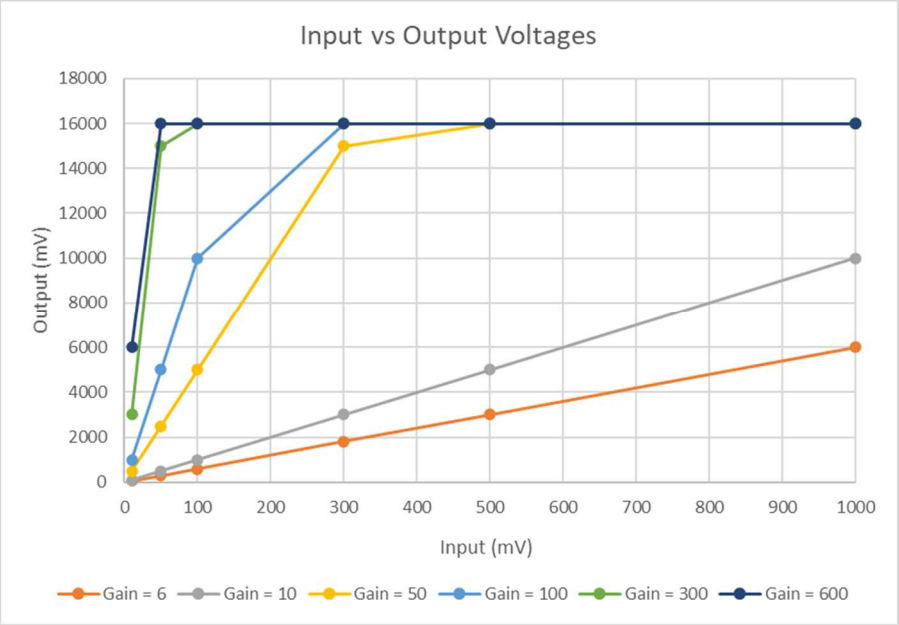

Fig. 4.1: Input Vs Output of 10 MΩ Impeded signal

Fig. 4.1 shows that the output remains linear at gain levels save for those in which the output signal meets or exceeds the rail voltage, 16 volts, of the operational amplifiers. Within the regions where the signal is not being amplified above rail voltage, the output is perfectly linear and matches computer simulated values. Additionally, input impedance did not have any kind of effect on the linearity of the gain. This is most likely due to the high sensitivity of the INA121PA operational amplifiers, boasting an input bias current of only 4 picoamps. This means that even with 100mV signal through 10 MΩ of impedance, the input current to the probe amplifier is 10 nanoamps, nearly 1000 times higher than the minimum sensitivity of the probes is capable of.

Settling time though was affected by both changes in input impedance and gain. As stated in the computer simulations models, the second cascading amplifier

of the input probe circuit is fitted with a small capacitor to correct overshoot, and as such settling time is determined predominantly by the rise time of the circuit.

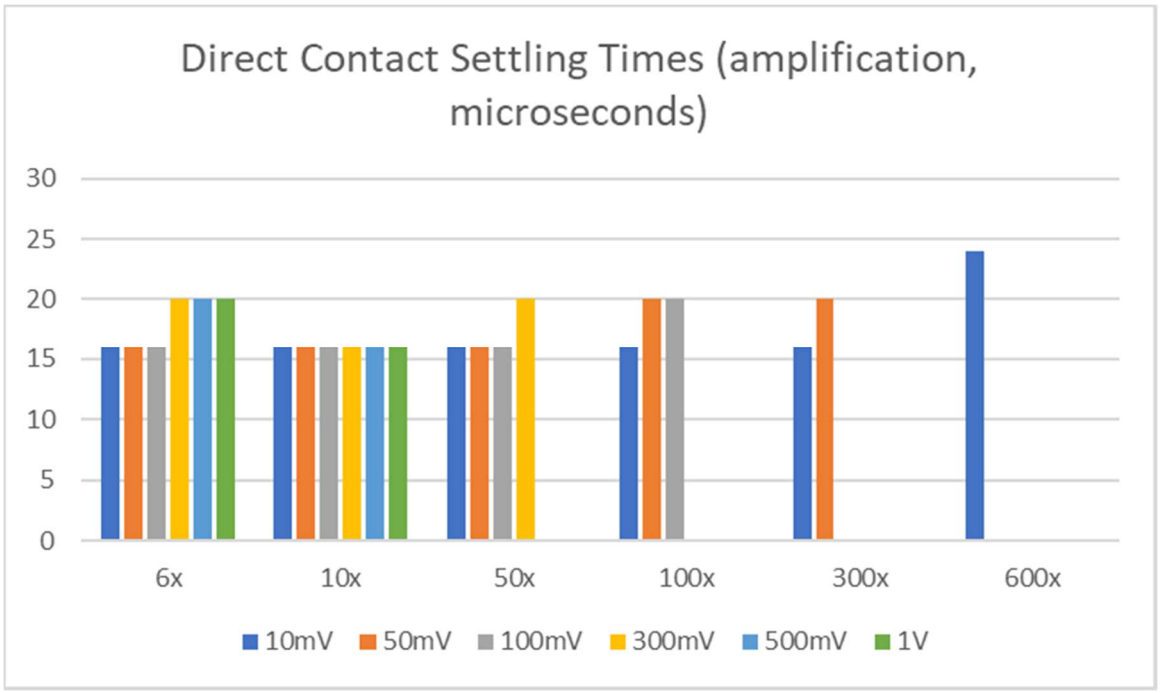

Fig. 4.2: Settling Times of Amplified Signal in Direct Contact with Function Generator

Fig. 4.2 demonstrates the settling time of the amplifier at varying inputs and gain levels. While in direct contact with the function generator, the settling times of the output signal average below 20 µS, with the exception of 600x gain of 10mV peaking at 24 µS.

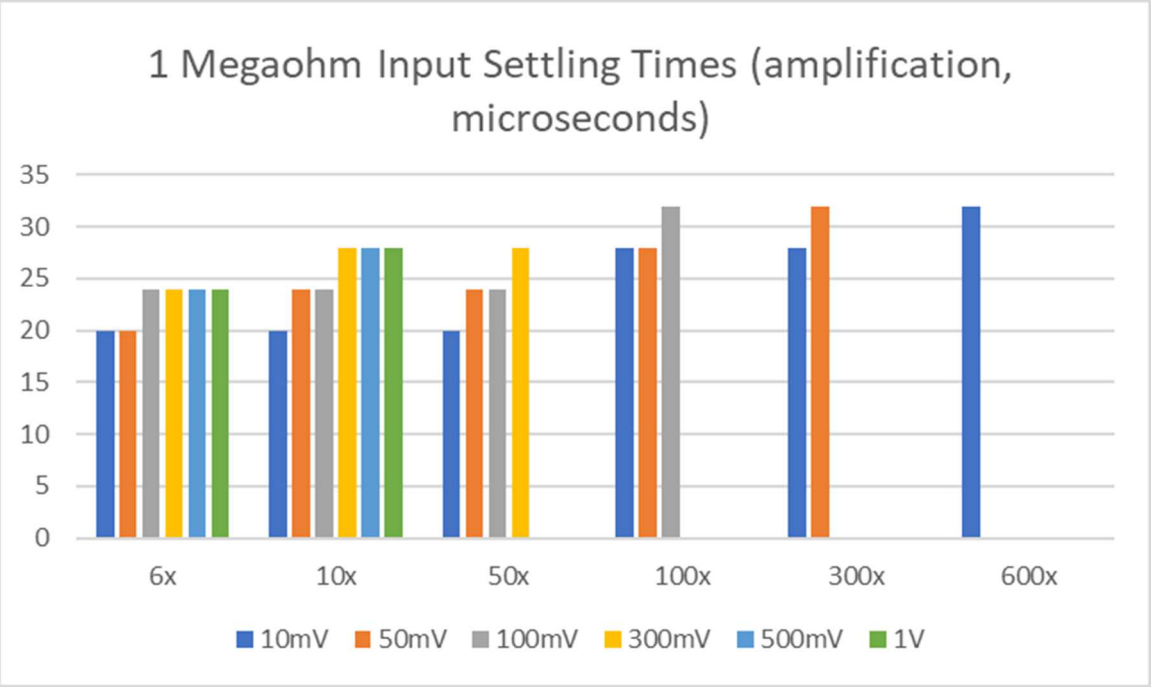

Fig. 4.3: Settling Times of Amplified Signal with 1 MΩ Impedance

Fig 4.3 Demonstrates that as input impedance goes up, settling time also increases and is far more affected by the input voltage. At this impedance value, settling time averages around 25 µS and peaks at 32 µS.

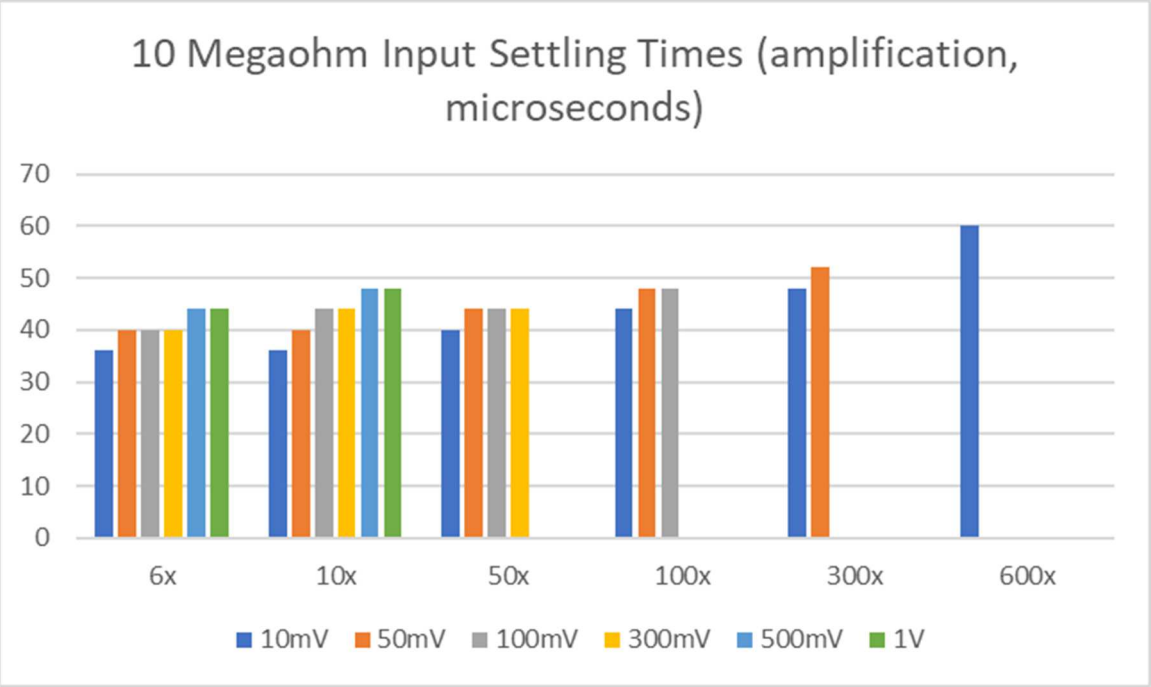

Fig. 4.4: Settling Times of Amplified Signal with 10 MΩ Impedance

The trend correlating increased input impedance and increases in settling time continues in Fig. 4.4. Average settling time at this level of impedance climbs to 45 μS and peaks at 60 μS. While this increase in settling time is nearly triple that of direct contact to the function generator, it is still a markedly smaller window of time that should be affected by biosignals. It should also be mentioned that at this impedance level, and at gain ratios higher than 100x, a small overshoot of about five percent above final settled output values is observed, which could be part of the cause for the increase in settling times. As stated in a previous section, the average impedance of probes used for biosignal acquisition such as tungsten or silver/silver chloride electrodes average between 5 to 8 MΩ, so it should not be expected that settling times of tissue measurements should exceed 60 μS.

Lastly, a signal to noise ratio was calculated to ensure that a low noise threshold could be maintained at varying gain. Given that all tissue experiments would occur while the amplifier circuit was held within a faraday cage, noise calculations are also gathered as such. Signal calculations are done by supplying a 10mV signal at 1 KHz 600x gain. Ambient noise values are gathered by grounding the reference electrode and leaving the input electrode connected to the function generator while it was not supplying any signal. At this gain level, the average noise of the system was within 1mV of oscillation. This is largely due to the extremely low noise capability of the LT1115 operational amplifiers used in buffering and filter stages boasting a noise ratio of 0.9nV/√Hz per the datasheet. This means that even for the 1 KHz signal the noise generated by the system would be 90nV, or less than 10% of the measured noise. This low noise floor is also due in part to the application of a 5 KHz filter at the final output stage of the circuit and the use of the faraday cage, both of which substantially reduce environmental noise.

For voltages, signal to noise ratio, or SNR, is calculated as follows:

$$\square\square\square = 10 * \square\square\square(\square - \square)$$

Where S represents the maximum amplified signal voltage, and N represents the measured output noise voltage at this gain level. This equation leads to a calculated signal to noise ratio of 86.99dB. This value is extremely crucial to the proper capture and amplification of a bioelectric signal, and as such a high SNR like this allows for proper measurements when testing on living tissues.

Outputs of Tissue Test Experiments

To understand how a device like this might function within the context of measuring living tissue, several experiments are performed on both nerve and cardiac tissue. Firstly, a mouse phrenic nerve was dissected and placed in a bath of buffered saline solution. A silver/silver chloride electrode was placed onto one end of a nerve pinned into a dish to prevent tissue movement. Then the nerve was mechanically stimulated 20mm away.

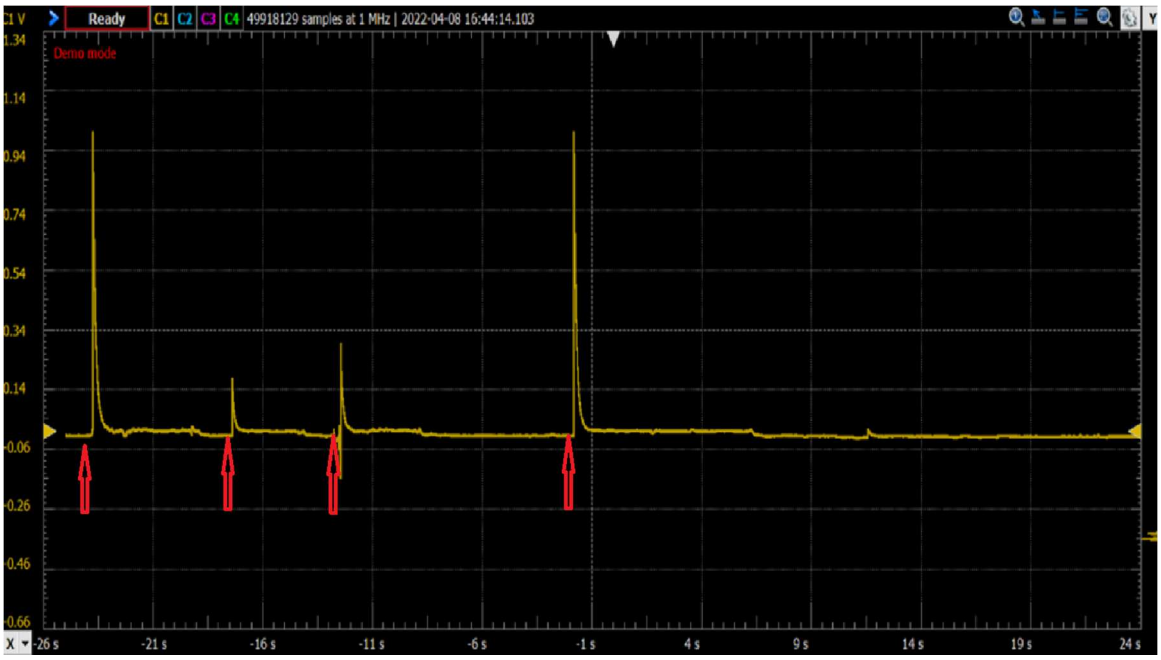

Fig. 4.5: Mouse Phrenic Nerve Tissue Measurements

Fig. 4.5 demonstrates the results of this test. All of the red arrows mark the instance where mechanical stimulation is applied. Spikes observed are extracellular electrical events caused by the mechanical stimulation of the nerve and measured by the electrode on the other end of the tissue length. After the fourth spike, a part of the tissue not containing the nerve was also stimulated to

ensure that the detected signal was not caused by strictly mechanical disturbance of the tissue.

To ensure that the measurements of the nerve test demonstrate a clear acquisition of bioelectric signal, a similar test was conducted by placing a silver/silver chloride electrode directly into the left ventricle of a dissected mouse cardiac tissue. This tissue was placed in a cycling bath of krebs solution to encourage pacemaker activity.

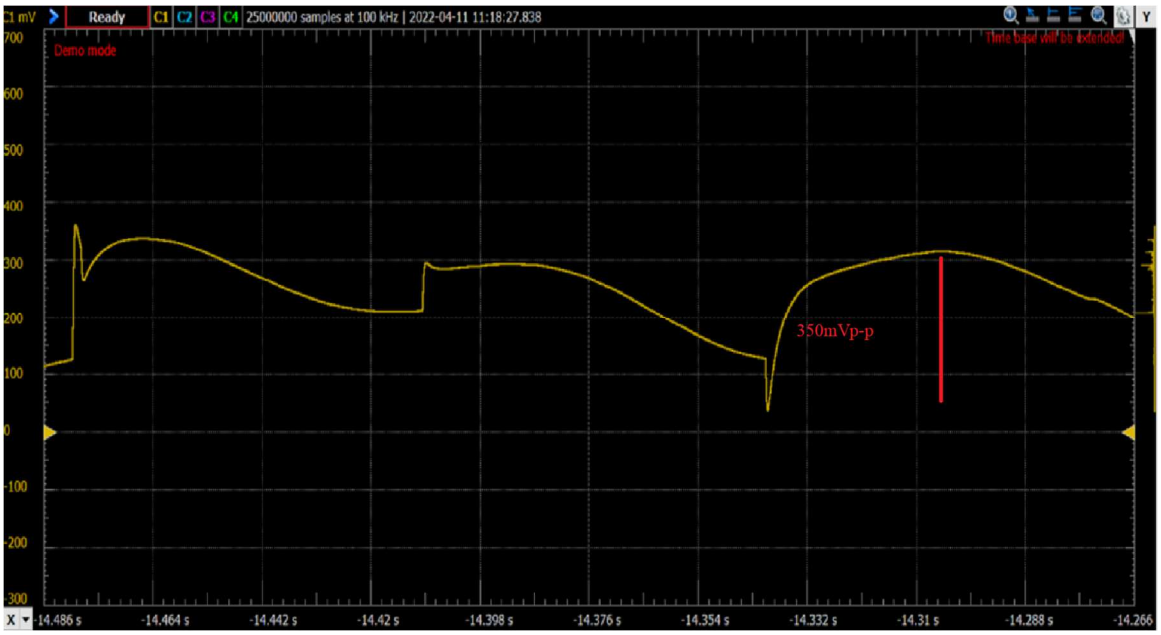

Fig. 4.6: Mouse Cardiac Tissue Measurements

Fig. 4.6 is the recorded extracellular measurement from this tissue, demonstrating a clear example of cardiac electrical activity. That being said, cardiac activity is not strictly electrical, and instead encourages mechanical movement within the tissue. To ensure that the measurements are not purely a

result of this movement, the drug Blebbistatin was used to prevent mechanical activity while allowing action potentials to propagate.

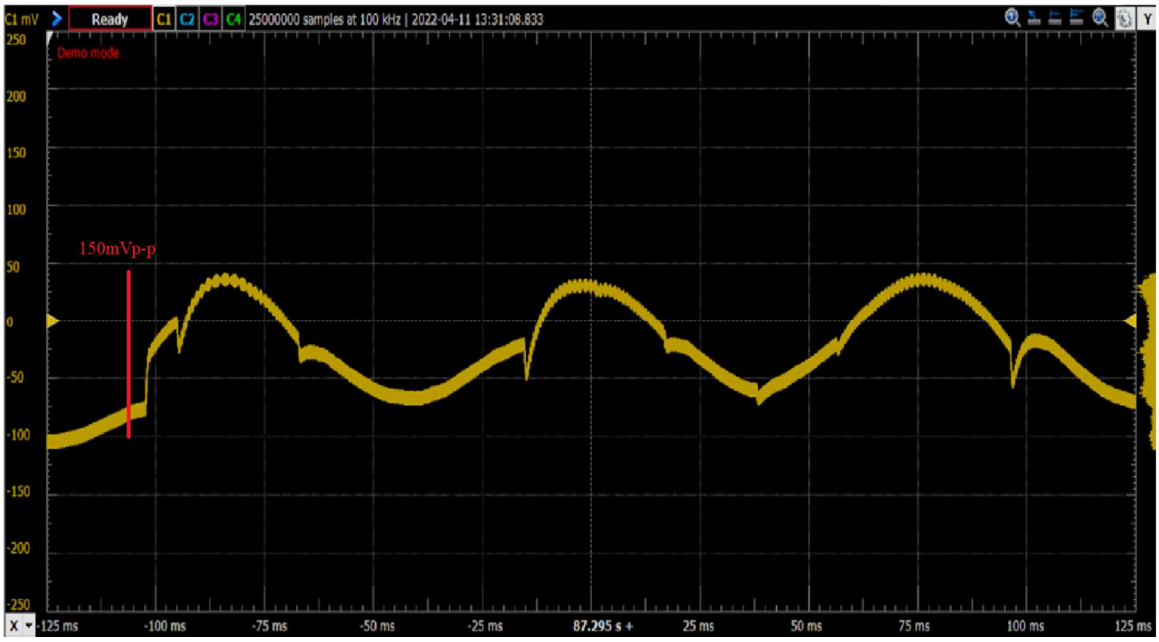

Fig. 4.7: Mouse Cardiac Tissue Measurements with the Addition of Blebbistatin

Fig. 4.7 is a recording of the extracellular activity within the ventricle after 20 minutes of exposure to Blebbistatin without changes to the gain of the system. It should be noted that while the action potentials are still very clearly defined, this experiment does demonstrate that the mechanical movement of the cardiac tissue does have an impact on the amplitude of the recording.

These tissue experiments demonstrate that the amplifier described in this thesis is capable of detecting and amplifying the electrical activity of living tissues to the extent that they can be used to modulate an optical diode.

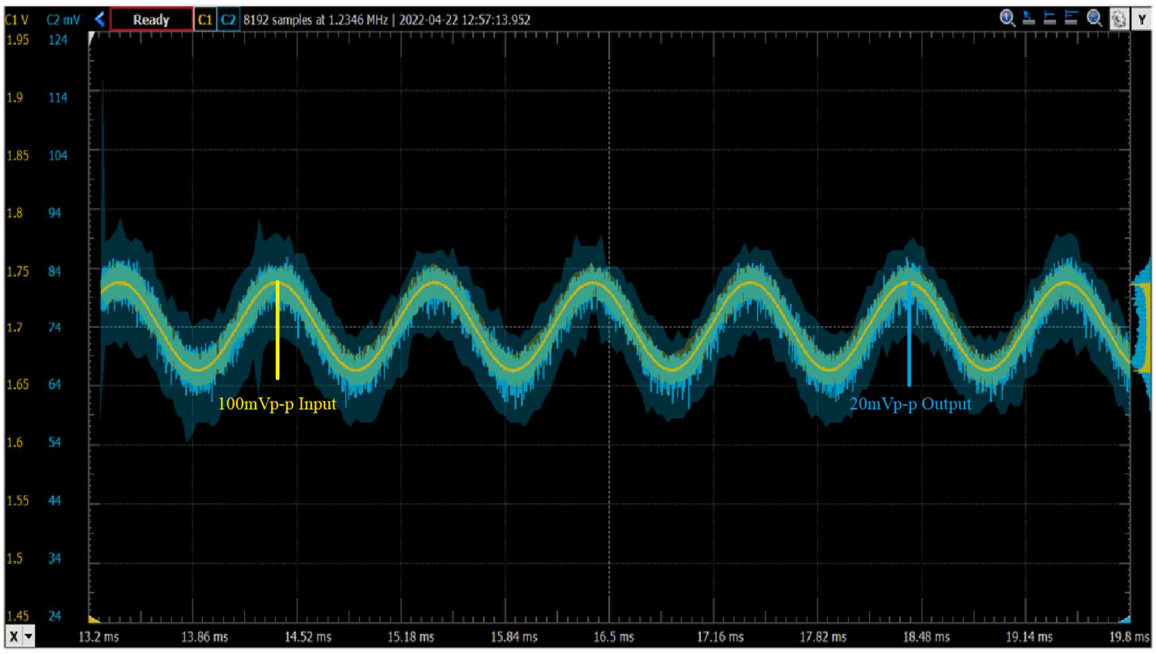

Fig. 4.8: Outputs of Optical Experiments at 1 KHz

A function generator is used to simulate the expected outputs of the amplifier based on the tissue results seen from both cardiac and neuronal measurements. These experiments utilize a 200mV peak-to-peak sine wave to simulate a realistically expected output signal voltage from the amplifier. The primary reasons for using a function generator are for consistency of signal, as well as for the simple addition of a 1.75V DC offset capable of putting the OD110LDS optical diode used in these experiments within its ideal range of functionality. Fig. 4.8 captures the 1 KHz wave encoded in by the change in optical output of the diode, and captured by the silicon detector on the other end of the optical tube setup. While this output wave only oscillates in the low mV range, this capture is also recorded without amplification to demonstrate direct output signal from the silicon detector.

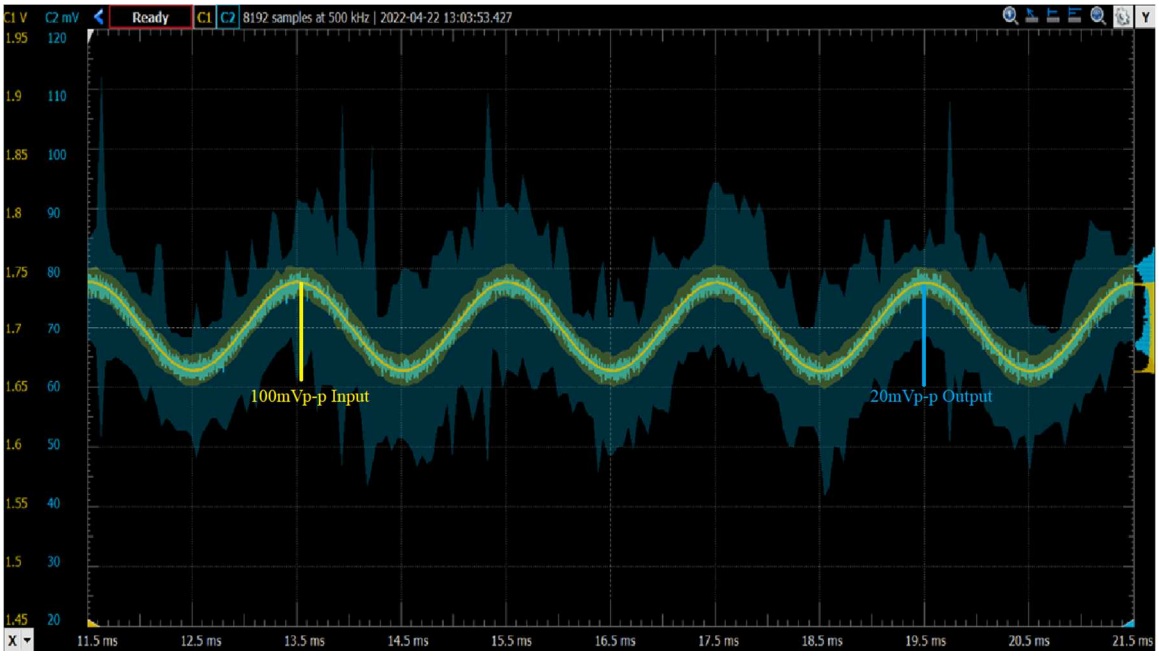

Fig. 4.9: Outputs of Optical Circuitry at 500 Hz

Fig. 4.9 is a captured measurement of the same testing setup as seen in Fig. 4.8, however the frequency is reduced to 500 to demonstrate that the optical system is properly encoding frequency information.

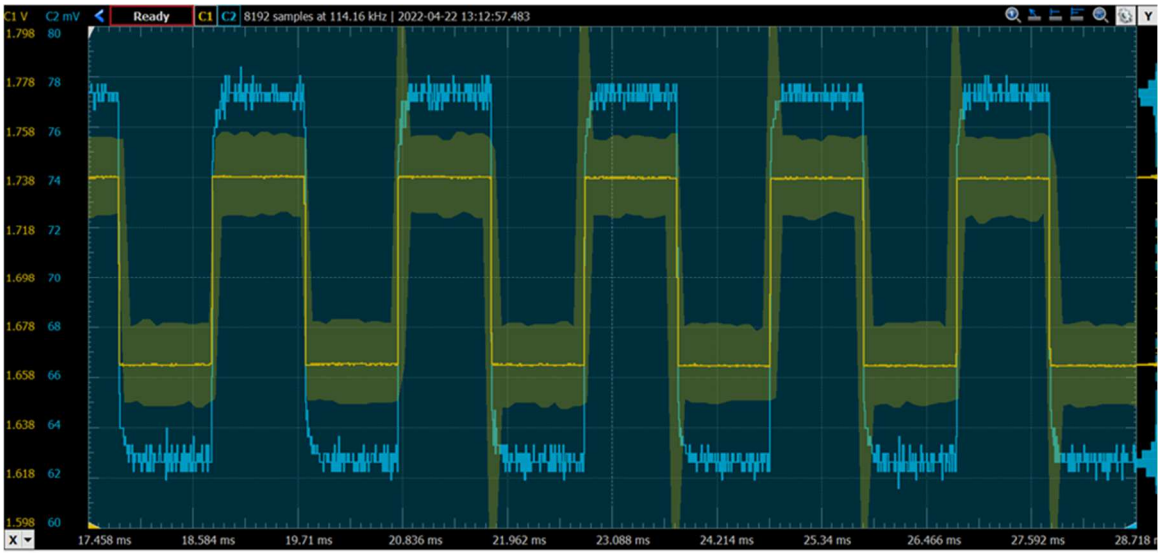

Fig. 4.10: Outputs of Optical Circuitry using 500 Hz Square Wave

Fig. 4.10 once again utilizes the same testing setup but with the use of a square wave input from the function generator in place of a sine wave. This experiment demonstrates that the process of optical conversion and deconversion is capable of preserving encoded waveform information as well. As with previous experiments, the same voltage drop is present and is not affected by changes to the waveform.

Discussion

Despite the increased settling time of the amplifier in the presence of high input impedance, the tissue measurements and measured voltage gain of the amplifier demonstrates an immediate capability for biosignal acquisition without substantial effects on the quality of the signal passing through the circuit. Additionally, the amplification provided by the circuit proves highly beneficial to the clarity of the recorded signal, as the passage of both frequency and waveform components to the proposed optical component are critical to the functionality of the diode used to modulate optical intensity and properly encode this signal along an optical medium.

The optical outputs also demonstrate a clear capability of encoding signals within the voltage output range created by measurements passed through the amplifier. The optical conversion described in this thesis proves capable of properly encoding all of the relevant information of biosignals for the purpose of passage along an optical medium.

It should be noted that the system has many areas in which function as an implantable device can be improved. Firstly, while the device is able to function on a rail voltage of only +/- 16V, substantially lower than commonly available bioamplifier systems, this voltage is somewhat impractical as an implantable device. This voltage was necessary for powering of the chosen operational amplifiers, however it also allows for a substantial range of headroom that is not fully utilized when measuring biologically generated electrical signals.

Additionally, the size of the amplifier used in this system would not be ideal for implantable device design. The dimensions of this amplifier are 3 inches by 4 inches on a nearly flat plane. While this is substantially downsized relative to most bioamplifiers, it is also far too large to be implanted in most places within a human body. This is mostly due to the use of through-hole construction operational amplifiers, chosen for their ability to be swapped easily in the event of chip failure or damage to any individual component.

Comparison of Simulated vs Experimental Results

The computer simulated results suggest a very high level of sensitivity and linearity as a bioamplifier. In practice, this is possible though only through specific means of measurement. In the first few rounds of experimentation, several electrode types are used to determine the capability of the circuit in properly gathering tissue signals. Copper and tungsten electrodes are used in tests attempting to gather signals from mouse small intestine and colon tissue to no avail. It was not until the silver/silver chloride electrode was created that tissue signals could be gathered in neuronal and cardiac tissue experiments.

Once the electrode had been implemented though, the measurements acted very similarly to expected values in regards to settling time and gain. It was not until the simulated input impedance tests that any changes in this settling time would become apparent, however as stated the settling time increase does not seem to have any substantial effect on signals that occur over the time frame action potential and electrical tissue signals are known to occur.

Chapter 5
Future Works and Conclusion

Future Works

In future iterations of this device, many new features should be implemented in the interest of expanding the number of tissue types capable of interfacing to this device. Firstly, variable filter stages could allow for extremely fine tuning of the device to specific tissue requirements. While some tissue types create smooth, regular pulses, others may require the measurement of more complex waveforms documenting the individual actions of specific ion channels or other complex electrical behavior within membranes.

In regards to the optical component, several improvements can be made to help further downsize the size of the optical driver. The core function of the device relies on the modulation of optical intensity through a focusing lens, and the experiments performed in this thesis utilized many components that would not be ideal for implantable conditions. The lenses used in this experiment had a focal length of 50mm, requiring more than 100mm for each lens enclosure to properly function. Other lenses can be used with substantially smaller focal lengths to help further downsize the device in the future. Additionally, the lenses each had a 10mm diameter which could also be substantially reduced in future versions.

Lastly, future versions of this device would go through proper surface mount production allowing for the placement of substantially smaller components, combination of printed circuit boards into one unit, and the development of better enclosures more suited to bodily implantation.

In the future, optically driven circuits could prove to be hugely beneficial for implantable device design in many areas of tissue research. Any electrically active tissue types could utilize a calibrated device utilizing the mechanisms of this device and passed out of the body using thin optical fiber to easily accessible data collection points along the body with minimal interference to bodily function. Additionally, the use of optical signaling prevents interference from other areas of electrically active tissue, preventing interference and allowing for an even higher degree of tissue measurement accuracy and clarity in densely packed tissue regions.

Conclusion

Optical technologies continue to expand each year, and their advancements in the field of biomedical devices could prove hugely beneficial for the reasons outlined above. As optical fiber continues to grow smaller and the manufacturing practices improve, new fiber designs can be introduced that allow for common use in bodily devices. Optical modulation circuitry is also something that can be downsized further, including the use of smaller, lower power LEDs and low noise transistor amplifiers.

Future developments could also lead to the development of two-way optical communication, allowing not only for the measurement, but stimulation of electrically active tissues. In this scenario, optically coupled devices could become the primary design for systems such as optical nerve bridging devices, as well as pacemaker systems that utilize optical fiber in place of traditional metal electrodes susceptible to bodily interference. Two-way devices could also be utilized to both stimulate and measure said stimulated responses of pacemaker tissues in the body to allow for fine tuning of artificial pacemaker devices in the heart and stomach, leading to the fine tuning of individual patient tissue responses in real time by medical technicians and doctors to specific needs.

Optically coupled devices also pose an interesting possibility for optical stimulation devices. Certain types of tissues like those found in the small intestine, can be stimulated by exposure to particular wavelengths. These sorts

of simulations could be regulated or controlled by the presence of exposed LED outputs from a device similar to the one described in this thesis.

From a diagnostic perspective, optically coupled devices could also be used for long-term tracking of tissue activity. These devices could drive a network of particular-wavelength LEDs placed carefully along long tissue measurements. These LEDs pass a light wave capable of traveling out of the body for real time monitoring of extracellular activity like slow waves as they pass along larger lengths of tissue for medical professionals to measure in real time.

The benefits of optically coupled implantable devices are just beginning to be explored, and the research performed here proves the concept that bioelectric signals are capable of being amplified and optically converted in real time. With this knowledge in mind, the possibilities for device applications increase dramatically and open a new world of possibilities for the field of biomedical device design as a whole.

References

[1] Åke Bernhard Vallbo, “Microneurography: how it started and how it works,” *Journal of Neurophysiology,* Vol. 120, Iss. 3, pp. 1415-1427, 2018.

[2] T. Mano et al, “Microneurography as a tool in clinical neurophysiology to investigate peripheral neural traffic in humans”, Clinical Neurophysiology, Vol. 117, Iss. 11, 2006.

[3] Lawrence Stark, Jose Negrete-Martinze, Guillermina Yankelevich N., George Theodoridis, “Experiments on Information coding in nerve impulse trains”, Mathematical Biosciences, Vol. 4, pp. 3–4, 1969

[4] Abraira, Victoria E, and David D Ginty. “The sensory neurons of touch,” Neuron vol. 79, Iss. 4: pp 618-639, July 2013.

[5] D.M. Wilson, W.J. Davis, “Nerve Impulse Patterns And Reflex Control in the Motor System of The Crayfish Claw,” Journal of Experimental Biology Vol. 1, Iss. 43, pp. 193–210. October 1965.

[6] A. Mark Evans, Christopher N. Wyatt, Nicholas P. Kinnear, Jill H. Clark, Elisa A. Blanco, “Pyridine nucleotides and calcium signaling in arterial smooth muscle: From cell physiology to pharmacology,” Pharmacology & Therapeutics Vol. 107, Iss. 3, pp. 286-313, March, 2005.

[7] Rudolf R, Khan MM, Witzemann V, “Motor Endplate—Anatomical, Functional, and Molecular Concepts in the Historical Perspective.” Cells, Vol. 8, Iss. 5, pp.387, 2019.

[8] Pujitha Weerakoon, Eugenio Culurciello, Youshan Yang, Joseph Santos-Sacchi, Peter J. Kindlmann, Fred J. Sigworth, “Patch-clamp amplifiers on a chip,” Journal of Neuroscience Methods, Vol. 192, Iss. 2, pp. 187-192, 2010.

[9] Kaiser, Gerd, Optical Fiber Communication 4th Edition, New York: McGraw Hill Publications, 2011.

[10] Sontheimer H., Ransom C.B., “Whole-Cell Patch-Clamp Recordings. In: Walz W., Boulton A.A., Baker G.B. (eds) Patch-Clamp Analysis”. Neuromethods, Vol 35. 2002.

[11] E T McAdams, J Jossinet, “Tissue impedance: a historical overview,” Physiol. Meas. Vol. 16, Iss. 1, 1995.

[12] Gaston A. East, M. A. del Valle, “Easy-to-Make Ag/AgCl Reference Electrode,” Journal of Chemical Education, Vol. 77, Iss. 1, pp.97, 2000.

[13] Mancini, R, “Op Amp Stability and Input Capacitance,” Texas Instruments, Dallas, Texas, 2005.

[14] Sanders KM. “Spontaneous Electrical Activity and Rhythmicity in Gastrointestinal Smooth Muscles”. Advances in Experimental Medical Biology, Vol 11, Iss. 24, pp.3-46, 2019.

[15] Dixon, Rose Ellen et al. “Electrical slow waves in the mouse oviduct are dependent upon a calcium activated chloride conductance encoded by Tmem16a.” Biology of Reproduction, Vol. 86, Iss. 1 pp. 1-7, January, 2012.